

June 14, 2018

Dear Editor,

We thank the reviewers for their comments. In the rebuttal letter, we addressed each reviewer's comments separately. The reviewers' comments are italicized, followed by our point-by-point response to the reviewers.

Enclosed please also find a copy of the revised manuscript with changes highlighted.

Sincerely,

Tiange Xing

Anonymous Referee #1

1/ Introduction

The manuscript by Xing et al. entitled "Generating porosity during olivine carbonation via dissolution channels and expansion cracks" reports on a very nice piece of experimental work on the in-situ hydrothermal carbonation of olivine aggregates. Careful attention is paid to the real-time development of microstructures to unravel reaction-induced porosity changes and fracturing. Indeed coupling and feedbacks between dissolution/crystallization and generation of new fluid pathways within mineral aggregates (synthetic rock) is still poorly known although highly relevant to metamorphic and alteration reactions which involve aqueous and carbonate fluids. The study basically confirms a reaction-transport-deformation model that has been proposed by the same authors in 2016 based on a very similar experiment using the same characterization technique. The difference with the present study mostly relies on the use of a different mineral grain size. The high similarity between the two studies makes sometimes difficult to distinguish between data that have been collected here and in the previous study. Naming samples like LGC (larger grain cup) and SGC (smaller grain cup) would potentially help.

Thank you for the suggestion! We adopted the name SGC for the fine-grained cup and LGC for coarse-grained cup in the revised manuscript.

2/ General comments

- 2.1 About Reaction progress

Estimate of the overall reaction progress in the cup is an important piece of information. In a system that is prone to porosity clogging due to volume expansion of the solid phases, it is expected that the nature, density and geometry of fluid pathways will change with reaction progress. Basically, are the features described in this study relevant to peridotites that are at the beginning of the carbonation process (< 10%) or do they apply to extensively carbonated systems?

A key finding of this study is the porosity generation mechanism that couples dissolution and precipitation during olivine carbonation. At the beginning of the reaction, it is conceivable that dissolution plays an important role in maintaining porosity. As reaction progresses, non-uniform expansion of the rock due to precipitation could lead to fractures (reaction-induced fracture). Once the host rock is fractured, accelerated reaction takes place to achieve 100% carbonation.

We added the discussion in the revised manuscript (line 453-456).

Basically, if one considers a solid volume (V_s) expansion of x , then the volume expansion of the solid matrix (ΔV_s) is a function of reaction progress (R): $\Delta V_s = V_s^0 R x$. Let consider the endmember case where the overall sample volume (V_r) is constant and that the expansion of the solid matrix is only compensated by porosity shrinking. Then, porosity will vanish when $\Delta V_s = V_r(p^0)$ where p^0 is the initial porosity. Finally, we end up with $R = p^0/(1-p^0)x$. In the SGC cup, $p^0 = 0.1$. Assuming $x = 0.4$ (40% solid volume expansion) then $R = 0.3$. We see that for reaction progress above 30% in the cup, porosity could have potentially vanished at constant sample volume.

Obviously, the constant volume assumption does not hold in the present case but this simple calculation shows why knowledge of the reaction progress is conceptually important.

Following this idea, the knowledge of the three parameters, sample overall volume expansion, average porosity and reaction progress when the experiment is terminated would be very useful.

The knowledge of the overall reaction progress is also important if the experiment is run in a close system (technical point to be clarified) the source of CO_2 will be limited. In a forsterite sample with 10% porosity, all the CO_2 initially supplied as $NaHCO_3$ will be consumed after 20% reaction progress.

We agree that the reaction progress is an important parameter. To quantify the extent of reaction using the microtomography data, the volume increase of the reaction products (i.e., precipitation) and/or the volume decrease of the original olivine grains (i.e., dissolution) must be evaluated. Unfortunately, the phase contrast between these solid phases (i.e., precipitants vs. olivine) is very small, and at the current spatial resolution of ~ 2 micron, numerous attempts failed to segment precipitants from olivine grain (i.e., the uncertainties were larger than the volume change). Even at the sites where large orthorhombic crystals are present, it is difficult to determine the phase boundaries between olivine and orthorhombic crystals. Improved imaging techniques and perhaps different experimental designs are needed to quantify the reaction progress.

We added a discussion to clarify this point (lines 302-303).

- 2.2/ About the Model

I see an alternative model to the stretching-induced fracturing model. The inner cup contains loose grains and the porosity is the highest there. Accordingly, most of the solution is located there, solution which, furthermore, can be partially renewed if the system is not fully close (inlet capillary open, technical point to be clarified). The dissolution activity is therefore expected to concentrate at the inner cup interface in the SGC sample. Indeed, sample cup grains may dissolve faster than loose grains due to their smaller grain size.

Could what the authors call stretching-induced fractures, be merely a localized dense network of dissolution features? Dissolution features will exhibit a different geometry in LGC sample where dissolution kinetics is expected to be smaller. According to this alternative model, reaction progress in SGC should be higher than in LGC for a given run duration, is that the case?

First, we want to clarify that the pore fluid was connected to a syringe pump at the upstream and to a pressure regulator at the downstream. A constant pore pressure of 10 MPa was maintained throughout

the experiments. This experimental setup can be considered as a semi-open system. We added this information in the revised manuscript (lines 141-143)

Now, it is possible that dissolution is more rigorous at the inner cup interface of the SGC sample. However, we don't think that the observed fractures are merely a localized dense network of dissolution features because we observed intense stretching-induced fractures at the outer surface of the cup as well (see Zhu et al., 2016). The sample was jacketed by a silicone tubing (to separate the pore fluid from the confining fluid) where the porosity between the cup's outer surface and the jacket is smaller than the porosity of the cup wall. So if dissolution is the main mechanism responsible for the intense fractures observed in the SGC cup, little fracturing should be expected at the outer surface of the cup, opposite to the observations. We agree that dissolution is a contributing factor, but dissolution alone could not fully explain the fracture locations and patterns observed.

Furthermore, if dissolution is the main mechanism, one should expect fracturing to occur earlier in SGC sample because of its smaller grain size. This is not what we observed. Although it is difficult to make a rigorous comparison of the reaction progress in SGC and LGC samples, the fact that fractures in LGC appeared within 30 hours of reaction whereas no fractures were observed in the SGC sample until after ~65 hours of reaction is not consistent with the dissolution kinetics.

- 2.3/ About the Application to Nature

In peridotites, olivine grain size is rather large (hundreds of μm). Is the LGC experiment with little stretching-induced fractures the most relevant to natural settings? In nature, the high porosity zone can be the one with the smallest grain size (e.g., cataclastic fault zone) what will happen then? I generally find that the implication for natural cases is not sufficiently discussed. Consequently, the reader has sometimes the feeling that the proposed model only applies to the described experiments with their specific design.

The mechanical strength and cohesion are critical parameters in the brittle failure criteria (for example, Coulomb-Mohr criterion). There are no universal correlation between rocks' grain size and their mechanical strength and cohesion, so there is no simple extrapolation that links LGC or SGC samples to natural peridotite. Both SGC and LGC are much weaker compared to natural peridotites, and SGC is considerably stronger than LGC.

Laboratory experiments are not capable of simulating natural settings because of the vastly different length and time scales. So we focus on identifying and gaining physical understanding of the underlying mechanisms. In Zhu et al. (2016) we proposed that non-uniform expansion could be an alternative mechanism for the reaction induced fracturing in systems where crystallization force is not sufficient to break directly the host rock. In this study, our goal is to further test this idea as well as discovering other mechanisms (e.g., dissolution). Our contribution is to bring forth experimentally verified mechanisms that may operate in nature and thus help unravel the complex natural processes.

We added a brief discussion in the revised manuscript (lines 453-458).

3/ Specific comments

L48: The notion of « olivine mineralization » is unclear. I understand "formation of olivine from a fluid" whereas I believe that the authors mean "formation of carbonates from olivine". Would not "CO2 mineralization" be more appropriate here?

We made some literature search and found that ‘olivine carbonation’ appears most frequently. We now changed “olivine mineralization” to “olivine carbonation”.

Section 2.1: There are a couple of unclear issues with respect to the experimental set-up. Did the authors use a top cap made of sintered olivine as in the 2016 paper? Does the confining pressure also apply to the sample top and bottom (no deviatoric stress?)? Is the solution isolated from the inlet capillary during experiment or is the system open in order to buffer the pore pressure? This is an important issue since it defines whether the experiments have been performed in a close or (semi)open system.

Yes, sintered olivine lids made from the same material as the cup were used in both SGC and LGC experiments. A small axial end load is applied independently from the confining pressure by locking the axial piston at a fixed position. Changes in the sample length during reaction could lead to some variations in the axial stress. The planar fractures observed in LGC, for example, could be affected by the reduction of axial load due to may be The fractures in SGC are unlikely to be associated with the differential stress because the fracture pattern is not consistent with stress-induced cracks.

The upstream was connected to a syringe pump to keep a constant pore pressure of 10 MPa. The downstream was regulated by a pressure regulator. So the experiments can be considered semi-open. We added the information in the revised manuscript (lines141-143).

Section 2.1: The authors mention that they use forsterite. Is that San Carlos olivine, please clarify, since it would define the amount of ferrous iron that is present in the system.

We used pulverized San Carlos olivine as the starting material to synthesize the olivine cups. The loose olivine grains are also San Carlos olivine. This has been clarified in the revised manuscript (lines 128-129).

Section 2.1: Can the authors exclude that drilling the aggregate to fill it with olivine sand grains may induce micro-cracks in the inner cup wall that will further localize dissolution features? Does cooling of the aggregate after sintering can induce thermal micro-cracks (nano-tomography characterization of the cup before running the sample?)?

Yes, we are certain that the fractures observed are not from the mechanical (drilling) or thermal (cooling) manipulation during sample preparation. For both sample, we performed several 3D scans, 1) before confining and pore pressure was applied, 2) after pressures were applied but at room temperature; 3) during temperature increase from 23-200C; 4) immediately after reaching the desired pressure and temperature conditions. No micro-cracks or fractures were observed in any of these scans in both SGC and LGS experiments.

L125: The present experiment only differs from the 2016 one by the change in the grain size of the sintered olivine poly-crystal that forms the cup. The importance of increasing the grain size of the cup olivine grains to approach the grain size of those located inside the cup should be more emphasized in the introduction section since it justifies writing a new paper !

We modified the text to emphasis the grain size investigation using LGS (lines 105-112).

L234: “Edge”, I suppose the authors mean inner edge of the cup according to Fig. 6 in the 2016 paper. Please clarify.

“Edge” here refers to the near surface of the cup wall. We have modified the sentence (line 387)

Section 3.3 and 3.4: It is not always clear in these two sections whether the authors are describing features belonging to LGC, SGC sample or both? Please clarify.

We adopted the names SGC and LGC and modified the text to clarify.

Section 3.3b: Dissolution features occur to be planar and perpendicular to the vertical z-axis (Fig. 6b & 9b). Is that related to the sample geometry, stress distribution? Are they expected to develop as such in rocks? This geometry of the dissolution features is not really discussed in the manuscript although they are the only macroscopic features that generate porosity in the sample (LGS) produced in the present study.

The LGC sample is mechanically weak, so it is conceivable that the dissolution of olivine could break the weak bonding and initiate the fracture. The planar nature of the fracture suggest that the propagation of the fracture is likely caused by mechanical load (in contrast to chemical load). It is possible that the axial compressive stress is lower than the radial stress in the LGS experiment. We also could not rule out the possibility that this planar fracture is dictated by the defect in the sintered sample. It is clear that this planar fracture in LGC is NOT induced by the non-uniform expansion. The grain size contrast is necessary for causing the non-uniform expansion.

We modified the text to clarify these points (See sections 3.1 and 3.4).

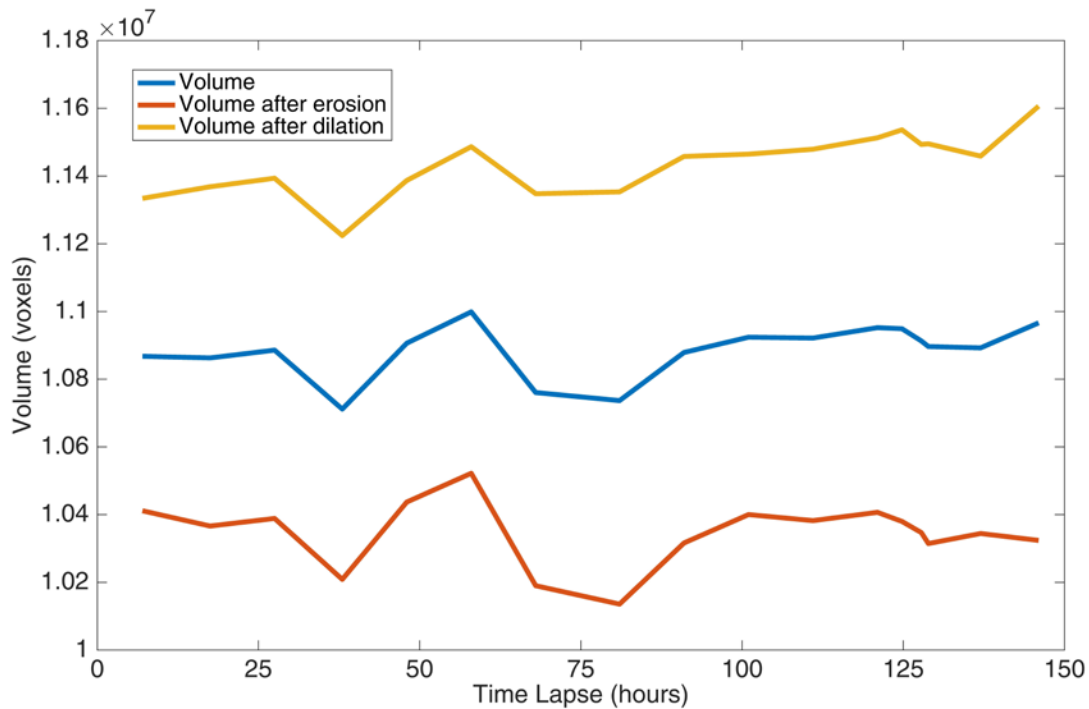
L287: “became dominate” should be “became dominant”?

Corrected.

L277-288: The grain size fluctuations described in this paragraph are fascinating. If I understand correctly, the size evolution of several grains has been monitored although only the size variation of a selected grain is displayed in Fig. 12. The possible link between local grain dissolution after 68h and development of fracturing in the cup is highly interesting. It would however be useful to see the size evolution of more than a single grain (what seems to be possible according to the available dataset?) to strengthen the inference. Would it also be possible to give error bars on the volume data to emphasize the significance of the observed variations?

We only selected the single olivine grain presented in Zhu et al. (2016) on which changes of the volume of magnesites are significant since segmenting one relatively large grain from the image is a process that require time and intensive work.

The volume of the grain is directly measured from the segmented olivine grain from inside the cup. The error of the volume measurement would only come from touching of other grains which is insignificant amount. We used the “erosion and dilation method” commonly used in image analysis to investigate the error that could be induced by spatial resolution. Results from the erosion and dilation does not change the trend of volume change presented here.



Section 4.1: It is unclear to me what data from this study supports the notion that the tubes pierce through the whole grains (holes), could not they just remain pits.

From the 3D analysis of the nanotomographic data, some tubes have clear bottoms inside the grains, but others form through-going holes across the whole grains. Since we do not see any precipitation filling or clogging the tubes, it is reasonable to think that these features represent different stages of tube formation. They started as the etch-pits. At the pits site, enhanced dissolution takes place, and the pits grow deeper and eventually become the through-going tubes.

We clarified this point in the text (lines 290-293)

L331: “Our quantitative estimates indicate that in these experiments, crystallization pressure can lead to maximum ~5% volume expansion”. Is not that estimate an average value of the volume expansion over the whole sample whereas reaction crystallization-pressure induced fracturing should be regarded as a volume expansion at the local scale? Please clarify.

Here the “crystallization pressure” means the mechanical force produced by the chemical reaction. We modify the sentence to clarify this point: “Our quantitative estimates indicate that in these experiments, the maximum volume expansion is ~5%.”

L331: I suppose that this assertion relates to the LGC, what is the volume expansion estimate for the SGC experiments where crystallization-pressure induced fracturing is also ruled out by the authors?

This above volume expansion estimate is for the SGC experiment. For the LGC experiment, no detectable volume expansion is observed.

Anonymous Referee #2

General comments:

This manuscript presents an experimental carbonation of olivine aggregates and the real-time observation of the reaction using in-situ dynamic X-ray microtomography and nanotomography. It builds on a previous study by the same group (Zhu et al., 2016) in which the authors reacted a cup made up of sintered fine-grained olivine (0-20 μm) and searched for dissolution, precipitation, and fracturing evidences. Here, the authors re use these data, perform more advanced investigations, and run a new experiment using coarse-grained olivine (80-100 μm). The main consequence of the olivine grain size difference is that precipitation of magnesite is spatially heterogeneous in the fine-grained experiment while it is homogeneous in the coarse-grained experiment. In the fine-grained experiment, the heterogeneous precipitation of magnesite produces a differential volume increase between the interior (maximum increase) and the nearsurface (no increase) of the cup walls so that the near-surface domains are fractured.

This leads the authors to suggest that reaction-induced fracturing occurs during carbonation and helps maintaining the reactive surfaces in olivine on short time scales.

The recognition of dissolution pits (etch pits) and channels indicates that dissolution could be the process maintaining the reaction on the long term.

Overall, the manuscript presented by Xing and coauthors is well written, presents interesting observations leading to logical conclusions, which make it a valuable contribution.

The experimental setup uses modern technics (in-situ dynamic x-ray microtomography and nanotomography) that bring novel observations on carbonation reaction. I suspect the data processing to be heavy and to require a lot of work and efforts, which makes this study even more valuable. I therefore recommend this manuscript for publication, provided the authors clarify a few points that I detail in the following.

Specific comments:

1) This study uses previous work from Zhu et al. (2016). I assume, but am not completely sure, that the authors simply used the data already acquired and did not run a new experiment using fine-grained olivine aggregate. Is that correct? In any case, Paragraph 3.2 could be slightly modified to emphasize more clearly which part of the observations and data processing is from Zhu et al. (2016) (then in theory not the best situated in a Results section but this is not a problem here) and what is completely new.

The microtomography experiment on the fine-grained olivine cup is the same as in Zhu et al. (2016) but the 3D analyses of fracture network, quantification of grain volume and porosity are new. The nanotomography experimental results (dissolution pits and tubes) on the reacted fine-grained cup are completely new.

Zhu et al. (2006) hypothesized that large grains would be preferred sites for precipitation of new crystals, Thus the loose olivine grains (100-500 μm) in the immediate vicinity of the inner cup surface (made of fined-grained, 1-20 μm , olivine) function as precipitate traps and thereby kept precipitation level at the surface of the olivine cup wall low. This led to the contrast in magnesite precipitation within the cup wall.

Because the grain size contrast played a key role in generating non-uniform volume expansion, we do need to compare the results of the fine-grained experiment (Zhu et al., 2016) to the new coarse-grained

experiments. To make the points clearer, we now use abbreviations SGC (for the fine-grained experiment) and LGC (for the coarse-grained experiment) at another reviewer's suggestion.

We have edited the text and made the new results more explicit.

2) Regarding the experimental setup, I guess there was a lid of olivine aggregate on the cup as in Zhu et al. (2016)? It may be worth mention it and represent it in Figure 3. Do the authors have an idea of the fluid flow direction in the cell? Is it purely vertical or does the more porous core (loose olivine sand) involve lateral flow through the cup walls? It may be of interest to explain and understand magnesite precipitation or nonprecipitation in the different domains.

We modified Figure 3 to add the lid.

These were not flow-through experiments. A constant pore pressure of 10 MPa was kept during the experiment. The pore fluid does not flow because there was no pore pressure gradient along or across the sample. The whole sample assembly was fully-saturated.

We added this information in Section 2.1 (lines 141-143).

3) The authors report a 10% initial porosity of the cup wall (line 129). Is it identical in the two cups? I wonder what makes this porosity, is it olivine grain boundaries or fractures? How interconnected is this porosity? I would suggest adding a short paragraph describing the structure of the starting aggregate.

The initial porosities of the two aggregated are similar, estimated from the microtomographic scans (see new Figure 8). From these scans, the pores the coarse-grained aggregate are fully connected, whereas the pores in the fine-grained aggregates form different connected clusters. This might also be partly because of that some of the pore throat are beyond the resolution of the microtomographic data. Both aggregates are very permeable, indicating well-connected pore networks.

We added more descriptions of the starting materials in the text (lines 128-138).

4) This is of importance because I do not completely get the distinction between the fracture and the dissolution planes, particularly the lines 239-243 and the Figures 5 and 6. For the reaction-induced fractures, do they cut across the olivine grains (i.e., breaking them in two) or do they use the grain boundaries? I have the same question for the dissolution planes. I also wonder why dissolution would form a single flat plane and not an anastomosing network. What causes the dissolution plane to have this geometry? Can we imagine that the size of the olivine grains plays a role, favoring large-scale, single structures (e.g., what is described as a single dissolution plane) in the coarse-grained experiment and small-scale, network-like structures (e.g., what is described as a crack pattern) in the fine-grained experiment?

The reaction-induced fractures cut through cluster of grains. Because the spatial resolution in the microtomography experiments is ~2 micron, and the reaction-induced fractures occur only in the fine-grained sample (0-20 micron), we are not able to resolve whether the grains were broken in two, most fractures developed using grain boundaries. Nanotomography data show that some fractures also cut through the olivine grains.

The Figure 9 (now Figure 10 in the revised manuscript) shows that the dissolution plane is primarily a single feature with a few small branches. Development of such secondary features are probably limited by the reaction duration (30 hours).

We think these fractures are dissolution-assisted fractures under tri-axial extension. We explained the formation of the planar features in the text:

“Under a constant confining pressure, volume reduction in olivine grains (i.e., dissolution) likely shortened the LGC sample length as reaction proceeded. Because the axial piston was kept at a fixed position during the experiment, this shortening in sample length resulted a decrease in axial stress. Because the LGC sample is mechanically weak (less cohesion), even though the reduction in axial stress is small, it could be sufficient to cause fracture LGC in the manner of dilation bands under triaxial extension (e.g., Zhu et al., 1997). Detailed examination of the 3D images revealed the disappearance of small grains along the plane which is clear evidence of dissolution. Thus we refer to these planar cracks as dissolution-assisted fractures under triaxial extension. The dissolution-assisted fractures were not observed in the SGC sample because it is much stronger owing to its fine grain size (e.g. Eberhardt et al., 1999; Singh, 1988). The triaxial extension stress condition would be no longer present once precipitation started (after ~36 hours) and sample volume expansion took place.”

5) The last part of the discussion focuses on the application of the findings to natural systems. I think this could be improved by discussing more how the results compare with observations made on natural samples. For instance, in the last paragraph, the authors state that reaction-induced fracturing helps maintaining the reaction on the short term while dissolution does it on the long term. There is one study on natural samples that could reinforce these conclusions. Reaction-induced fracturing has been recognized in peridotites serpentized at mid-ocean ridges by Rouméjon and Cannat (2014, G3). The hydration leading to the replacement of the olivine by serpentine occurs along a network of fractures (forming the so-called mesh texture). These fractures develop in two steps: 1) conjugate fracture planes of combined tectonic and thermal contraction origin that crosscut the olivine before hydration; 2) reaction-induced fractures associated to the volume increase consecutive to serpentinization while hydration occurs. It is shown (see their Figure 8c) that the reaction-induced fracturing occurs in the early stages of serpentinization (probably before 20% of serpentinization) while the rest of the volume increase is accommodated by the serpentine itself and dissolution processes dominate until completion of the reaction.

Many thanks for the suggestion and we also really appreciate the reference. This could be an important direction for the future work.

We added new discussion on the relevance of the laboratory experiments and field studies (lines 450-458).

6) Another question to develop concerns the typical length scale of the dissolution and fracturing processes. In this study, such processes occur at nano- to micrometer scales (Lines 291-2923: “micro-meter scale in the case of the coarse-grained aggregate and at nano-meter scale in the case of fine-grained aggregate, and reaction-induced fracturing in the case of the fine-grained aggregate.”). These scales are rather small for natural samples and would correspond to a second order permeability. Much larger permeability pathways (e.g., mm to cm cracks) are required to efficiently channel fluids and provoke carbonation of significant volumes at rapid time scales. Do the authors think their results are transposable at such larger

scales? And if so, could they make suggestions on what would it require for actual CO2 sequestration? (e.g., system dimensions, typical grain size, . . .)

In this study, we focus on understanding the underlying mechanism of porosity generation during olivine carbonation reaction. The physics of the porosity generation mechanism is scale independent. While the grain size used in laboratory settings are much smaller, the time scale using is also much shorter. It is conceivable that given enough time, the nano- to micrometer scale cracks could grow to centimeter fractures.

We do however, recognize that upscaling is always challenging for laboratory investigation. We added new discussion on the relevance of the laboratory experiments and field studies (lines 450-458).

7) Finally, I find Figure 12 intriguing and full of potential for further studies. This is a nice example of advances made possible by X-ray tomography in the comprehension of mineralogical reactions. I think there is still a lot of microstructural work possible using such technics.

We agree.

Technical corrections:

Lines 19-20: "dissolution fractures developed". I guess the authors mean dissolution planes?

Corrected.

Line 24: I would rephrase the end of this sentence: "by the volume mismatch in the cup walls, between the expanding interior and the near-surface that keeps a nearly constant volume"?

We have modified the sentence to clarify.

Line 32: Not sure Escartin et al. (1997) is the most relevant here. Maybe you could cite review papers such as Deschamps et al. (2013, Lithos) or Guillot et al. (2015, Tectonophysics) that list and discuss peridotite exposures

We have added the citation of Deschamps et al. (2013) in the introduction.

Line 78: "olivine mineralization" is unclear, needs clarification

We have modified this to olivine carbonation.

Lines 104-105: I suggest reformulation: "with larger grain size (80-100 μm) compared to the previous experiment reported by Zhu et al. (2016; 0-20 μm).

Modified.

Line 129: I guess the 10% porosity refers to the coarse-grained olivine aggregate. Is it comparable to the fine-grained olivine aggregate?

Both samples have an initial porosity of 10%. Also shown in the Figure 8, initial porosity of the two samples are comparable.

Line 133: I do not think the authors clearly mention the duration of their experiment. I suppose this is 36h for the coarse-grained experiment and 7 days for the fine-grained experiment (from lines 149 and 150)?

In the abstract they mention “until the olivine aggregates became disintegrated”. Is it really the case? It should be described here.

The clarification has been added.

Line 164: “simplified analyses” is a bit odd. I think I understand what the authors mean but that can be rephrased.

This phrasing has been modified.

Lines 168-169: “both the cup wall (surface?) and the cup (wall?) interior”

The sentence has been modified to clarify this.

Lines 187-189: Not sure this paragraph is really useful

We have modified the paragraph and also the structure of the section 3.

Line 191: “is not observed to be dominated by stress-generated fracturing” is a though formulation, needs rephrasing

Modified.

Lines 192-193: this should go in the discussion

We have incorporate that into the discussion.

Lines 193-195: Needs rephrasing, the sentence about the loose grains seems to be in the middle of two sentences talking about the cup walls. “precipitation-caused nonuniform stretching” is hard to follow.

Modified.

Line 195: “in the sample”. I guess the authors refer to inside the olivine aggregate as opposed to the surface. Throughout the manuscript, it is sometimes hard to follow what the authors are referring to due to the changes in the terminology (e.g., interior is also used to refer to the inside of the cup wall)

Modified.

Line 199: “as a single plane” instead of “along a main plane”?

Corrected.

Line 202: “disintegration of the cup’s wall”

Modified.

Lines 203-204: Maybe I am wrong, but “fragile” and “cohesion-less” seem to say the same thing here, so I suggest rephrasing

Modified.

Line 205: “after 68 hours of reaction”. “exhibits a hierarchical manner” is a bit odd, needs rephrasing.

Modified.

Lines 206-207: "Figure 5b shows that the fractures first occurred in areas close to the surface and propagated inwards. "The fracture first developed as a single. . .".

Modified.

Line 209: "systematic" can be deleted

Modified.

Lines 210-212: The end of the sentence is not clear and would need rephrasing. But it also looks like discussion and should be removed (as well as line 213).

This is a description of the fractures network pattern. Its morphology is similar to the 'mud desiccation crack'.

Line 215: "their", not really clear what it refers to

We have modified the sentence to clarify.

Line 216: cite Figure 8 here instead of at the end of the next sentence?

Added the citation.

Line 231: "a volume expansion"

Modified.

Line 241: "It's obvious". . .not really

A citation to Figure has been added here.

Line 242: "along"

Corrected.

Line 251: "exhibits a hierarchical geometry in which the fractures that appeared first are now the largest"

Line 252: "domains" instead of "patches"

Modified.

Line 262: Is there a way to have typical sizes (e.g., diameters) or it is too variable?

The typical radius of the ~6 pixels (360 nm). We discussed the radius in the estimation of the permeability in discussion. Statement on the inner diameter of the tubes has been added here.

Line 326: I would add a reference here, as in the introduction (line 51)

Line 360: "should still be in a range"

Corrected.

Line 422: "and the resulting contrast in the expansion" is unclear, needs rephrasing

The statement has been modified to clarify.

Figure 1: “reacted” and “unreacted” are not clearly visible, change the color Lines 579-580: the sentence is complicated, needs reformulation

Modified.

Figure 4: It took me a while before understanding where the subvolume 2 was exactly positioned. It gives the impression that the subvolume 2 was outside of the cup. Perhaps a 2D sketch would be more efficient.

We changed the shading to better illustrate the cubes. The 2D representation of subvolumes 1&2 could be found in Zhu et al. (2016).

Figure 9: If possible, add the orientation of these volumes

We have added annotation to indicate the cup’s outer and inner surface (now Figure 10).

Figure 10: To which experiment and time does this figure correspond? Also, I could understand that the dashed line polygon corresponds to the upper half of the photos but it was not straightforward. I suggest indicating that differently (e.g., annotate the upper half of the photos or modify the orientation picture).

We have added in the figure captions the names SGC for the fine-grained sample and LGC for the coarse-grained sample.

We modified figure capture to better describe the dashed lines (new Figure 11).

Anonymous Referee #3

The manuscript presents experimental results for carbonation of olivine in 4D, three spatial dimensions plus time. It is a follow-up on a previous paper from the same group (Zhu et al., 2016), and provides both some additional data on the experiment in the previous paper and results from a new experiment using a coarser-grained initial material. There is not much 4D data on such processes available in the literature, which makes this a topic that is suitable for publication, within the scope of the journal, and will attract a lot of attention. The paper is also well written and fairly easy to read, although there are some misprints.

However, in my opinion the authors are spending too much time on repeating statements and data that is already present in Zhu et al. (2016). Of course some background information from the previous paper needs to be included, but quite large parts of the text can be removed and replaced with a reference to Zhu et al., and perhaps more importantly, repeated background information should be clearly marked as being repeated, to avoid giving the fake impression of being new data presented in this manuscript. Furthermore, there is not that much information about the new coarse-grained experiment, and it would be a lot more interesting to see some more details about the differences between the fine-grained and coarse-grained experiments instead of an extended discussion of the crack patterns presented by Zhu et al. Thus, I recommend a major revision where the authors should reduce the amount of repeated data. In the following I firstly give my recommendations for what should be removed, and suggest some other data that could be included. Then I list a few major concerns, followed by some minor comments and a list of misprints.

We made a major revision in Section 3. Detailed changes are listed below.

Remove or add

- Section 3.2 is mainly repeated from Zhu et al., and should be shortened significantly.

There is no need to repeat the entire description of the formed cracks and cemented patches, since the interested reader can look up Zhu et al. instead. Figure 7 is a direct repetition from Zhu et al., but I admit that this might be useful to include as background.

The grey value distribution in figure 8 is also included in Zhu et al., although in the supplementary material and without the best fit representation. If the authors include the same type of analysis on the coarse-grained experiment, this would be interesting, but without it I don't see much value in the figure. In the end of the section the authors estimate the expansion, something Zhu et al. didn't do, apart from noting that the material expanded. It is fine to include this number here, but it would be more interesting with a similar number from the coarse-grained experiment. The expansion might be zero in that case, but if so it should be stated clearly. Furthermore, is it possible to extract expansion as function of time from the data? That might be interesting.

We have reorganized the section 3 and to make our new result more explicit. Paragraphs and figure that might be considered a repetition have been removed from the section.

For the grey value histogram, we have now included our analysis on the LGC sample in the new Figure 7.

The expansion is not observed in the coarse-grained experiment. We have clarified this in the revised paper (lines 226-227).

- Section 3.4 would be more useful if it compared data from the fine-grained experiment with similar data from the coarse-grained experiment. As it is, this section is mainly a more verbose version of what is already written by Zhu et al., with a few additional estimates of growth rate.

This section is modified in the revised manuscript (lines 265-287)

- Section 4.2 is a large chunk of the discussion, and mainly repeats stuff from Zhu et al., and most of it can be removed. Also, figure 13 can safely be removed. Although it shows 3D data and Zhu et al. only presented a 2D plot, the data here is hard to interpret and only discussed in context of 2D porosity distribution. Thus, it has little value. A few comparisons between the two experiments might be interesting, but not much more.

We do think that it is important to visualize the 3D porosity distribution (now Figure 14). The figure provide an easy visualization that 1) the porosity reduction as a result of precipitation is non-uniform (with smaller porosity at the center); 2) there is no detectable secondary porosity generated in the region where most precipitation takes place. This is the key difference between the "crystallization pressure model" and the "volume mismatch model".

We modified the section4.2 in the revised manuscript.

Major concerns

- In figure 6, it is stated that the linear feature in the coarse-grained aggregate is caused by dissolution. It is not at all clear to me why dissolution would cause such a linear structure. In a flow-through experiment you might expect some sort of wormholing, but this can hardly be relevant here. Rather, I would assume that what is shown is a single axial crack, with secondary dissolution of the crack faces. If the authors really think the structure is just caused by dissolution, they have some explaining to do as to why this ends up

being linear. Some data on formation of this crack-like structure in time and perhaps tracking of grains at each surface of the structure might help. Now this is just guessing, but I think such a structure might be caused by a crack if you have less, but non-zero, volume expansion in the coarse-grained aggregate. Higher volume change would naturally then lead to a denser crack pattern. Of course there is some dissolution going on, but I have a hard time understanding why it would organize itself as a crack.

Thanks for pointing this point.

We agree that these fractures are axial cracks, with secondary dissolution of the crack faces. They are renamed as “dissolution-assisted fractures under tri-axial extension”. We explained the formation of the planar features in the text:

“Under a constant confining pressure, volume reduction in olivine grains (i.e., dissolution) likely shortened the LGC sample length as reaction proceeded. Because the axial piston was kept at a fixed position during the experiment, this shortening in sample length resulted a decrease in axial stress. Because the LGC sample is mechanically weak (less cohesion), even though the reduction in axial stress is small, it could be sufficient to cause fracture LGC in the manner of dilation bands under triaxial extension (e.g., Zhu et al., 1997). Detailed examination of the 3D images revealed the disappearance of small grains along the plane which is clear evidence of dissolution. Thus we refer to these planar cracks as dissolution-assisted fractures under triaxial extension. The dissolution-assisted fractures were not observed in the SGC sample because it is much stronger owing to its fine grain size (e.g. Eberhardt et al., 1999; Singh, 1988). The triaxial extension stress condition would be no longer present once precipitation started (after ~36 hours) and sample volume expansion took place.”

- I do not believe that the “expansion cracks via stretching” mechanism is a reasonable full explanation of the cracks. On lines 231–233 the authors state that grains in the center of the cup wall move apart. Now, these grains were initially bonded mechanically. How can they separate if these bonds are not broken during the process?

Clearly they must be. This might be caused by some sort of dissolution-precipitation creep or by reaction induced cracking. I guess it would be difficult to tell the difference based on the available data, but to me it seems likely that these bonds are at least partly cracked, before the crack is recemented by the reaction products. Thus, there might be dense, invisible cracking in the center of the cup wall, while the effect of this cracking and expansion in the wall center is a less dense crack pattern on the outside of the cup wall. A rock simply cannot expand in a chemical process that involves dissolution of the base material and precipitation of some product unless bonds between the initial grains are broken. Uneven heating of a rock would cause something like the situation presented in figure 14, with the yellow part being warmer than the green, but in a chemical process there has to be some deformation in the reacted part.

The microtomographic images clearly show a volume expansion in the center of the cup wall where there is no evidence of cracking or porosity increase. So we think that the expansion is more likely resulted from a dissolution assisted creep process, not by fracturing caused by crystallization pressure.

The main point of Figure 15 is that in a system where the crystallization force is not large enough to directly fracture the host rock, if the volume expansion (by creep) is heterogeneous within the sample, reaction-induced fracturing and porosity increase can still occur as a result of stretching caused by the volume mismatch.

We modified the text to clarify this point (lines 444-450).

Minor comments

Generally, please state more clearly in figure captions whether results are from the fine-grained or coarse-grained experiment.

We have added in the figure captions the names SGC for the fine-grained sample and LGC for the coarse-grained sample.

Line 179: A description of the color scale used would be helpful, e.g. something like "... where X represents black, and Y is white".

This is a statement of the binarization process. We convert the image into the phase of interest (assigned value 1) and the matrix (assigned value 0).

In our data, the black to dark grey colors represent pores, and white to light grey colors represent olivine (illustrated in Figure 7).

Lines 264–266: Here, it is noted that there is evidence for hierarchical fracturing within the olivine grains. Later, it is peculiarly written on lines 333–335 that there is no evidence of cracks in olivine grains. This is at best sloppy. Furthermore, why are these cracks forming, if not by the very reaction induced cracking that the authors claim is not observed?

Thanks for pointing this out. The sentence (lines 333-335 in the original version) was modified:

"Indeed, the nanotomography data show only dissolution features such as etch pits and worm holes, with no evidence of crystallization pressure induced cracks (Figure 11)" (lines 368-370)

Lines 278–288, and figure 12: It would be interesting to see plotted the individual volume change of the olivine grain and the formed precipitates. I would also suggest changing the figure a bit, it is hard to see the structure of the precipitated material. Something closer to figure 5 in Zhu et al. would be better.

We made diligent attempts to segment the different solid phases (i.e., olivine vs. precipitates). Unfortunately, the phase contrast between the precipitants and olivine grains is very small, and at the current spatial resolution of ~2 microns, we could not segment precipitants from olivine grains with acceptable uncertainties. Even at the sites where large orthorhombic crystals are present, it is difficult to determine the phase boundaries between olivine and orthorhombic crystals. Improved imaging techniques and perhaps different experimental designs are needed to quantify the reaction progress.

We modified the figure (now Figure 13) to increase the contrast between olivine and precipitates.

Figure 1: The text "Reacted" is extremely hard to see, please consider changing the color.

Thanks for pointing this out. We have changed the color in the revised Figure 15.

Figure 5: Why is the dissolution or crack always in the lower right corner?

This is a mere coincidence. Dissolution features and cracks are also observed in other parts of the sample. Figures below show that this dissolution is also observed in other places rather than just the lower right corner.

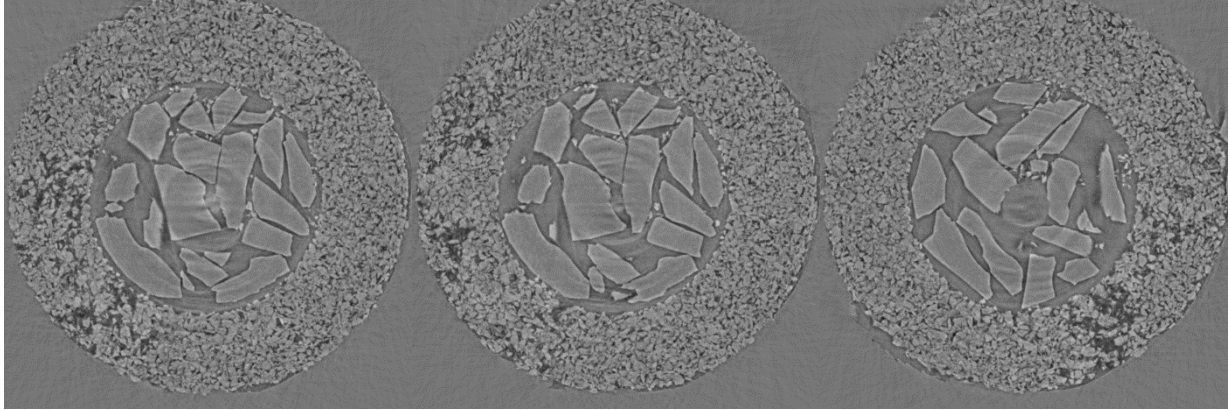


Figure 9a: I'm unable to interpret the fracture network, please consider reworking the figure a bit and perhaps include a view from different angles.

We have changed a viewing angle of the fracture network in Figure 9 (now Figure 10 in the new version of manuscript). We also partly changed the opacity of the fracture to better illustrate the structure.

Misprints

Line 38: reaction -> reactions

Corrected.

Line 92: system -> systems

Corrected.

Line 131 (and other places): x-ray -> X-ray

Corrected.

Line 154: images -> image

Corrected.

Line 206: shown -> shows

Corrected.

Line 232: gains -> grains

Corrected.

Line 242: alone -> along

Corrected.

Line 251: appeared -> appearing

Corrected.

Line 255 and figure 14 caption: none-uniform -> non-uniform

Corrected.

Figure 1: crystalization -> crystallization

Corrected.

Generating porosity during olivine carbonation via dissolution channels and expansion cracks

Tiange Xing¹, Wenlu Zhu¹, Florian Fousseis², Harrison Lisabeth^{1,3}

¹ Department of Geology, University of Maryland, College Park, 20742, USA

5 ² School of Geosciences, University of Edinburgh, Edinburgh, EH9 3FE, UK

³ Department of Geophysics, Stanford University, Stanford, 94305, USA

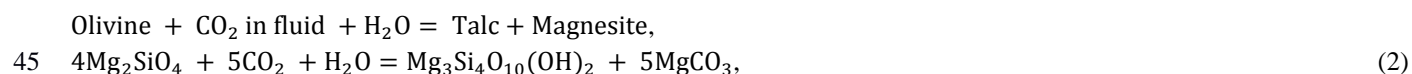
Correspondence to: Tiange Xing (tiange@umd.edu)

Abstract. The olivine carbonation reaction, in which carbon dioxide is chemically incorporated to form carbonate, is central to the emerging carbon sequestration method using ultramafic rocks. The rate of this retrograde metamorphic reaction is controlled, in part, by the available reactive surface area: as the solid volume increases during carbonation, the feasibility of this method ultimately depends on the maintenance of porosity and the creation of new reactive surfaces. We conducted in-situ dynamic ~~*X~~X-ray microtomography and nanotomography experiments to image and quantify the porosity generation during olivine carbonation. We designed a sample setup that included a thick-walled cup (made of porous olivine aggregates with a mean grain size of either ~5 or ~80 μm) filled with loose olivine sands with grain sizes of 100-500 μm. The whole sample assembly was reacted with a NaHCO₃ aqueous solution at 200 °C, under a constant confining pressure of 13 MPa and a pore pressure of 10 MPa. Using synchrotron-based X-ray microtomography, the 3-dimensional (3-D) pore structure evolution of the carbonating olivine cup was documented until the olivine aggregates became disintegrated. The dynamic microtomography data show a volume reduction in olivine at the beginning of the reaction, indicating a vigorous dissolution process consistent with the disequilibrium reaction kinetics. In the olivine cup with a grain size of ~80 μm (coarse-grained cup), dissolution ~~fractures~~planes developed within 30 hours, before any precipitation was observed. In the experiment with the olivine cup of ~5 μm mean grain size (fine-grained cup), idiomorphic magnesite crystals were observed on the surface of the olivine sands. The magnesite shows a near constant growth throughout the experiment, suggesting that the reaction is self-sustained. Large fractures were generated as reaction proceeds and eventually disintegrate the aggregate after 140 hours. Detailed analysis show that these are expansion cracks caused by the volume mismatch in the cup walls, between the expanding interior and the near-25 surface which keeps a nearly constant surface volume. Nanotomography images of the reacted olivine cup reveal pervasive etch-pits and worm-holes in the olivine grains. We interpret this perforation of the solids to provide continuous fluid access, which is likely key to the complete carbonation observed in nature. Reactions proceeding through the formation of nano- to micron-scale dissolution channels provide a viable microscale mechanism in carbon sequestration practices. For the natural peridotite carbonation, a coupled-mechanism of dissolution and reaction-induced fracturing should account for the observed self-sustainability of the reaction.

1 Introduction

Mantle peridotites are exposed widely on the Earth's surface in tectonic settings such as mid-ocean ridges, subduction zones and ophiolites (Escartín et al., 1997; Fryer et al., 1995). Peridotite is mainly composed of olivine which is unstable at temperature below 700 °C in the presence of water (Evans, 1977)(Evans, 1977), and below 500 °C in the presence of CO₂-rich fluids (Johannes, 1969)(Johannes, 1969). The transformation of olivine to serpentine and carbonates due to fluid-rock

interaction is extensively observed in peridotite outcrops (e.g. [Beinlich et al., 2012](#); [Falk and Kelemen, 2015](#); [Hansen et al., 2005](#)); (e.g. [Beinlich et al., 2012](#); [Falk and Kelemen, 2015](#); [Hansen et al., 2005](#)). Rock deformation experiments have demonstrated that fluid alteration to peridotite can strongly affect the strength and tectonics of the oceanic lithosphere ([Deschamps et al., 2013](#); [Moore et al., 1996](#)). Therefore, study of the olivine-fluid interaction is of great importance in understanding the alteration process of peridotite in a variety of tectonic regions. General peridotite alteration ~~reaction~~ reactions can be formulated as follow (Hansen et al., 2005; Kelemen and Matter, 2008):



Although peridotite weathering reactions occur widely in nature, the rate of olivine ~~mineralization~~ carbonation at subsurface conditions is debated. Since the retrograde metamorphic reactions are kinetically fast, the extent of transformation is limited by fluid supply which depends on the accessible fluid pathways. As the hydration and carbonation of olivine results in an up to ~44% increase in solid molar volume ([Goff and Lackner, 1998](#); [Hansen et al., 2005](#); [Kelemen and Matter, 2008](#)); ([Goff and Lackner, 1998](#); [Hansen et al., 2005](#); [Kelemen and Matter, 2008](#)), carbonation of olivine is generally assumed to be self-limiting: the reaction products would gradually fill up the pore space and lead to a decrease in the porosity ([Emmanuel and Berkowitz, 2006](#); [Hövelmann et al., 2012](#)); ([Emmanuel and Berkowitz, 2006](#); [Hövelmann et al., 2012](#)), which in turn lowers permeability and reduces fluid supply. This negative feedback would ultimately force the alteration to cease. However, naturally occurring completely carbonated peridotites are evidence that these limitations can be overcome. For instance, listvenite is the natural completely carbonated product of peridotite, which is composed of magnesite, quartz and trace minerals ([Beinlich et al., 2012](#); [Nasir et al., 2007](#)). This creates a conundrum of how the large extent carbonation can be achieved with the potential self-limitation of reducing fluid pathways.

In order to explain this discrepancy between the theory and the observation, numerous studies have been conducted aiming to find a mechanism to maintain the access for reacting fluid during olivine alteration reactions. In 1985, Macdonald and Fyfe examined naturally altered peridotite and proposed that the large volume change associated with the reaction could generate high local stresses and strains, which would cause episodic cracking. This idea has then been applied to olivine carbonation by Kelemen and Matter (2008), who proposed a positive feedback loop where fractures could be generated during the volume-expanding reaction, porosity and permeability can be maintained or even increased, which in turn would accelerate the carbonation processes (cf. Rudge et al., 2010). In 2011, Kelemen et al. showed that in natural peridotites cross-cutting hierarchical fracture networks filled by syn-kinematic carbonate and quartz veins extend to microscopic scales. These cross-cutting networks indicate coeval carbonate crystallization and fracturing. Several studies also showed that the forces generated by the volume increase should be enough to fracture peridotite ([Iyer et al., 2008](#); [Jamtveit et al., 2009, 2011](#); [Ulven et al., 2014](#)).

75 While reaction-induced fracturing is accepted as a way to maintain fluid access, the mechanical details of the process are poorly understood. As for the mechanism that generates stresses, ‘crystallization pressure’ (also termed ‘force of crystallization’) has been proposed (e.g. Scherer, 2004; Weyl, 1959; Winkler and Singer, 1972). In this model, the precipitation/crystallization of reaction products exert pressure around the growing crystals, and fracturing takes place when that pressure exceeds the local minimum principal stress (Kelemen and Hirth, 2012). Salt crystallization (Scherer, 2004) is a common example where high crystallization forces due to the nucleation of precipitates in pore space cause samples to ‘burst from the inside’ (see Figure 1a). However, studies have shown that the crystallization force is low in the olivine carbonation system (e.g. van Noort et al., 2017). Because of the lack of experimental evidence of crystallization forces during olivine alteration, Zhu et al. (2016) proposed an ‘expansion cracking’ mechanism as an alternative model after successfully producing reaction-induced fractures in an in-situ synchrotron X-ray microtomography study. In the ‘expansion cracking’ model, tensile stresses are generated due to the volume mismatch between regions with different precipitation rates, leading to cracks forming in regions that expand slower than their surroundings (see Figure 1b).

85 Beyond fracturing, dissolution has been recognized as an important part of the olivine alteration process (e.g. Velbel, 2009; Velbel and Ranck, 2008; Wilson and Jones, 1983) and proposed as a mechanism to explain the observed complete carbonation of peridotite. In 1978, Grandstaff showed that dissolution could significantly increase the surface area through etch-pitting. Wilson (2004) suggested that the weathering of olivine is controlled by etch-pitting and channel formation due to preferential dissolution, which assists the migration of fluid and promote further reaction. Andreani et al. (2009) suggested that permeability may be maintained during peridotite carbonation by the development of preferential flow zones. Lisabeth et al. (2017a, 2017b) observed relevant structures in dunite samples that have been reacted under controlled stress conditions, and interpreted them as a pattern of secondary porosity bands formed by dissolution coupled to locally intensified compressional stresses.

95 Previous investigations of olivine carbonation were largely based on the interpretation of naturally deformed samples (e.g. Macdonald and Fyfe, 1985), thermodynamic modelling (e.g. Kelemen and Hirth, 2012) or comparison with reaction systems other than olivine (e.g. leucite to analcime in Jamtveit et al., 2009). While these approaches led to significant advancements, there are limitations to the understanding of the mechanisms responsible for porosity generation during olivine carbonation that these approaches can provide. The history of natural fault rocks is inevitably complex, and thermodynamic arguments and numerical models can only indicate a potential, while the actual progress of chemical reactions is strongly affected by interfacial structures, which vary considerably in different mineral systems. Thus, it is critical to complement such studies with laboratory experiments on olivine carbonation.

105 Synchrotron-based X-ray tomography is an advanced non-destructive method to capture three-dimensional images of materials. Where processes affecting these materials are followed through time, a 4-dimensional (3 spatial dimensions + time) dataset is captured. By using X-ray transparent reaction cells (Fusseis et al., 2014b), the technique enables the investigation of fluid-rock interaction at controlled and geologically relevant conditions. We examined the carbonation process of olivine on the basis of 4-dimensional images acquired by X-ray microtomographic imaging with synchrotron radiation at the Advanced Photon Source. Zhu et al. (2016) hypothesized that large grains would be preferred sites for precipitation of new crystals, and the contrast in the grain size produced the volume mismatch due to a preferred precipitation on the larger grains and led to the fracturing of the sample. To further test the hypothesis, in this current study, we conducted a new experiment using an olivine aggregate with larger grain size (80-100 μm) compared to the previous experiment reported by Zhu et al., (2016; 0-20 μm). We also performed advanced 3D analyses and quantification of the micro- and nano-tomography data obtained by Zhu et al. (2016). In an advancement of the results presented by Zhu et al. (2016), here we present direct evidence for the coupled mechanisms of dissolution and precipitation-driven fracturing during olivine carbonation and demonstrate their importance in

115 sustaining the reaction progress at different spatial and temporal scales. We further show direct evidence of how reaction-
induced fracturing operates, i.e. how stress is generated through volume-increasing reactions. A better understanding of olivine
carbonation directly applies to the geological sequestration of CO₂ (Gislason et al., 2010; Mani et al., 2008). The principle of
in-situ carbon mineralization is the conversion of silicate and hydroxide minerals to form carbonate minerals as a stable sink
for CO₂ (Power et al., 2013). Peridotite, because of its wide occurrence and high reactivity, is considered one of the best
potential feedstocks for CO₂ mineralization (Andreani et al., 2009; Beinlich and Austrheim, 2012); the estimated rate of CO₂
120 consumption peridotite carbonation could be as high as 2×10⁹ tons·km⁻³ per year (Kelemen and Matter, 2008). As the dominant
constituent of peridotite, olivine becomes the most important mineral for CO₂ mineralization. Our study provides new insights
into carbon sequestration using ultramafic rocks, and our findings on the mechanism of fracture generation during olivine
carbonation could provide guidance to industrial applications.

2 Experimental Setup

125 2.1 Sample Configuration

In Zhu et al. (2016), the contrast in grain size between the loose grains and the cup wall aggregate is hypothesized as the cause
of the non-uniform precipitation which is crucial to the generation of fractures in the experiment. Here, we use coarse-grained
olivine aggregate in the cup wall to reduce the contrast in grain size between the cup wall and the fillings and further test their
hypothesis.

130 The sample assembly consists of a millimeter-sized synthesized San Carlos olivine cup, filled with loose San Carlos olivine
sand (grain size 100-500 μm, see Figure 2a) and then covered by a lid made of the same material as the cup. Both the olivine
cup and its lid are taken from a sintered pellet made from pulverized San Carlos olivine with a grain size of 80-100 μm. This
coarse-grained olivine cup is referred to as large grain cup (LGC) in the following discussion. Data obtained from the LGC
experiment will be compared to the results of an olivine carbonation experiment conducted by Zhu et al. (2016) at the same
135 experimental conditions, on a fine-grained (grains sizes between 0-20 μm) cup. The fine-grained olivine cup is referred to as
small grain olivine cup (SGC) in the following discussion.

The cup, which was fabricated by hot-pressing in a procedure described in Zhu et al. (2016), has inner and outer diameters of
1 and 1.8 mm respectively, with a resulting wall thickness of 0.4 mm. ~~It has an initial porosity of 10%. ~0.4 mm. The initial
porosity of the cup is ~10%. Both LGC and SGC samples were sintered for 4 hours at 1400°C, the LGC sample came out
weaker (less cohesive) compared to the SGC sample, and the initial porosity of LGC is slightly higher than that of SGC.~~

140 The loose grains inside the cup allowed the inspection of magnesite growth on free olivine surfaces. The sample assemblies
(i.e., olivine cup + loose grains) were jacketed and loaded into an ~~X~~-ray transparent pressure cell (Figure 3). A confining
pressure of 13 MPa and a pore fluid of NaHCO₃ aqueous solution (1.5 mol·L⁻¹) at 10 MPa were applied to the sample. ~~The
pore pressure downstream is regulated by a pressure regulator while the upstream is controlled by a syringe pump to form a
semi-open system. Both upstream and downstream pore pressures were maintained at 10MPa throughout the experiment. A
small axial load is applied independently from the confining pressure by locking the piston at a fixed position.~~ The pressure
cell was then heated to 200 °C to initiate the reaction. These conditions were kept constant during the entire microtomography
experiment. ~~The reaction of the LGC sample was stopped at 36 hours after considerable secondary porosity generation was
observed. No magnesite precipitation was detected in LGC. The SGC sample was reacted for 7 days until intense fracturing
was observed. Significant magnesite precipitation was detected in SGC (Zhu et al., 2016).~~

2.2 Micro- and Nano-tomography

Third-generation synchrotron facilities produce electromagnetic radiation bright enough to allow rapid imaging even inside experimental vessels, thereby enabling studies of dynamic processes ranging over periods from seconds to days, while acquiring individual 3-dimensional (3-D) data sets in fractions of a second. Synchrotron X-ray microtomography has therefore become one of the most powerful tools in structural geology and rock mechanics studies (see Fuisseis et al., 2014a for a review and Bedford et al., 2017 for a recent application).

In this experiment, synchrotron-based X-ray absorption microtomography has been used to record the dynamic carbonation of olivine in 4 dimensions. We used an X-ray transparent cell (Fuisseis et al., 2014b), mounted in the upstream experimental station at beamline 2BM of the Advanced Photon Source of Argonne National Laboratory, 25 m from the source. There, a polychromatic beam filtered by 1 mm aluminum, 15 mm silicon and 8 mm borosilicate glass yielded a photon flux with an energy peak at 65 KeV (Zhu et al., 2016). A Cooke pco.edge sCMOS camera with 2560×2160 pixels (pixel size 6.5×6.5 μm^2) was used in a flying scan mode. The sample-detector distance was 300 mm, which introduced a clear phase contrast signal to the data (Cloetens et al., 1996). The camera recorded projections from a 10 μm thick LuAG:Ce single crystal scintillator, magnified through a 10× Mitutoyo long-working distance lens yielding a pixel size of 0.65 μm . Projections were collected with an exposure time of 50 ms while the sample was rotated over 180 $^\circ$ with 1.2 $^\circ\cdot\text{s}^{-1}$. 1500 projections were collected in 150 s. For the LGC sample, 115 3-D microtomographic data sets were acquired over 36 hours, together forming a 4D data set, with time as the fourth dimension. For the SGC sample, 379 data sets were acquired over 7 days. From these 379 datasets, 19 were chosen for further detailed quantitative analysis. All acquired microtomographic data were reconstructed using the code Tomopy (Gürsoy et al., 2014) into stacks of 2160 images each, with dimensions of 2560×2560 pixels per image. Each of these image stacks contains a 3-dimensional representation of the sample mapped onto a 32-bit image, with the grey values reflecting the local absorption of X-rays (Fuisseis et al., 2014a). Where the refractive indices change in the sample, i.e. on edges, this absorption signal is locally overlain by a phase contrast signal (Cloetens et al., 1996). The time series dataset covers the entire duration of the experiment.

After the in-situ acquisition of the microtomography images, a fragment of the cup wall from the SGC was taken to conduct nano-scale imaging. Nanotomography was conducted using a transmission X-ray microscope (TXM) at the beamline 32-ID of the Advanced Photon Source of Argonne National Laboratory. A monochromatic beam of X-ray with an energy of 8 keV was used. An X-ray objective lens corresponding to a Fresnel zone plate with 60nm outermost zone width was used to magnify radiographs onto a detection system assembly comprising a LuAG scintillator, a Zeiss 5X optical microscope objective lens and an Andor Neo sCMOS camera. Nanotomography yields a pixel size of ~60 nm after binning.

2.3 Image Processing Procedures

~~Zhu et al. (2016) conducted simplified analyses and measurements on 2-dimensional image slices (see Figure 2b) through the 3-D microtomography datasets of fine-grained aggregate acquired in this experiment. In this study, we present the results of a true 3-dimensional volume quantification of the microstructural changes in the sample (i.e., spatio-temporal changes in grain and pore volumes).~~

~~For the fine-grained aggregate, in each of the 19 reconstructed volumetric datasets Zhu et al. (2016) conducted preliminary analyses and measurements on 2-dimensional (2-D) image slices (see Figure 2b) of SGC through the 3-D microtomography datasets acquired. Here, we present the results of a true 3-D volume quantification of the microstructural changes in the SGC~~

sample (i.e., spatio-temporal changes in grain and pore volumes) and compared them with the results obtained from LGC sample in this study.

190 In both the SGC and the LGC samples, a sub-region that included both, the cup wall near-surface as well as the ~~cap~~cup wall's interior was chosen for detailed inspection. ~~Within that sub-region from all datasets. For each sample,~~ two subvolumes ~~(see subvolume 1 and 2 from Figure 4)~~ with athe dimension of $400 \times 400 \times 400$ voxels ($260 \times 260 \times 260 \mu\text{m}^3$) were cropped out from the region of interests in the cup wall in all datasets. ~~Subvolume~~(see Figure 4, subvolume 1 and 2 from SGC and subvolume 3 and 4 from LGC). In the SGC sample, subvolume 2 was further cropped to a volume of $247 \times 400 \times 400$ voxels ($160.55 \times 260 \times 260 \mu\text{m}^3$) to eliminate the boundary of the cup wall.

200 ~~Image segmentation is the separation and extraction of phases of interests from the 3D data sets for further analysis and quantification. A large range of segmentation algorithms exist (e.g. Kaestner et al., 2008). In global binary thresholding, images are segmented by identifying the grey value range representing a phase and assigning all voxels within that range a single value (usually 1) while all other voxels are classified as matrix (and assigned a different single value, usually 0) (Heilbronner and Barrett, 2014).~~ Image segmentation is the separation and extraction of phases of interests from the 3-D data sets for further analysis and quantification. A large range of segmentation algorithms exist (e.g. Kaestner et al., 2008). In global binary thresholding, images are segmented by identifying the grey value range representing a phase and assigning all voxels within that range a single value (usually 1) while all other voxels are classified as matrix (and assigned a different single value, usually 0) (Heilbronner and Barrett, 2014). Global binarization was conducted in Avizo Fire 8 to isolate pores from solids.

205 ~~At~~In the SGC sample, at the given spatial resolution, we could not resolve the new crystals precipitated within the cup wall and only the pore space was segmented there. Pixels with grey values that fall in the range $(-0.00031, -0.000077)$ were assigned to pore space. We used the segmented data to quantify the change in the spatial distribution of pores during the experiment. Each subvolume ~~(Figure 4)~~ was further divided into smaller cubes (side lengths $\sim 26 \mu\text{m}$) in which the average porosity is calculated to examine where changes in porosity occurred. In the LGC sample, grey values that fall in the range $(-0.00031, -$
210 $0.000095)$ were assigned to pore space.

In the nanotomography data, the grey value range between $(2.97672 \times 10^{-9}, 0.13161)$ was assigned to pore space. In these data, the olivine is represented by grey values between $(0.30846, 1.3161)$. Voxels with intermediate grey values $(0.13161, 0.30846)$ were assigned to reaction precipitates (e.g. magnesite).

3 Data analysis and results

215 ~~In our experiments, we~~We have observed the development of secondary pore spaceporosity during the reaction in both the ~~coarse and fine grained olivine aggregate experiment~~ LGC and SGC experiments (Figure 5). ~~However, detailed~~Detailed examination has further revealed the differences between the formations that the porosity generation in LGC is significant different from that in SGC.

3.1 Dissolution in the LGC sample

220 As reaction proceeded, olivine grains in the LGC sample shrank in size and secondary pores were produced (Figure 5a). This suggests that dissolution dominated the carbonation reaction in LGC, with little precipitation detected. The secondary pore space formed first at the center of the cup wall and grew outwards (Figure 5a), which is opposite to that in SGC where fractures grew from the surface of cup wall inwards (Figure 5b).

225 Planar fractures formed within 36 hours of reaction in LGC (Figure 6), and the experiment was stopped shortly after the formation of these pores/fractures. Because of the lack of precipitation, these planar fractures could not be induced by the non-uniform volume expansion as in the SGC sample (Zhu et al., 2016). Under a constant confining pressure, volume reduction in olivine grains (i.e., dissolution) likely shortened the LGC sample length as reaction proceeded. Because the axial piston was kept at a fixed position during the experiment, this shortening in sample length resulted a decrease in axial stress. Because the LGC sample is mechanically weak (less cohesion), even though the reduction in axial stress is small, it could be sufficient to cause fracture LGC in the manner of dilation bands under triaxial extension (e.g., Zhu et al., 1997). Detailed examination of the 3D images revealed the disappearance of small grains along the plane which is clear evidence of dissolution. Thus we refer to these planar cracks as dissolution-assisted fractures under triaxial extension. The dissolution-assisted fractures were not observed in the SGC sample because it is much stronger owing to its fine grain size (e.g. Eberhardt et al., 1999; Singh, 1988). The triaxial extension stress condition would be no longer present once precipitation started (after ~36 hours) and sample volume expansion took place.

3.2 Lack of precipitation in the LGC sample

Evidences from direct observation and quantitative analysis have shown that the LGC sample is lack of precipitation.

240 Within the duration of the reaction, hardly any precipitation was observed in the cup wall. In the microtomographic images, the surface layer of the loose olivine grains remained free of precipitates. Both sides of the cup wall remained straight and showed no spalling due to precipitation-caused non-uniform stretching. The sample did not experience any expansion as seen in the SGC sample.

245 Apart from the direct observation, grey value histograms of the data also show evidence of lacking precipitation in the LGC sample. The grey value histograms of 4D microtomography data evolve systematically during in-situ experiments, which can be utilized in ~~their~~the evaluation of the reaction progress (Fusseis et al., 2012). (Fusseis et al., 2012). Systematic analysis of the histograms of the grey value distribution revealed the progression of reaction during the experiment. ~~In our data, we observed~~ (Figure 7).

250 Comparing the histogram of SGC sample with the LGC sample, the shape of the histograms from the LGC sample (Figure 7a) is clearly asymmetric compared to the bell-shaped histograms in the SGC sample (Figure 7b). The slope on the precipitation side of the LGC histogram is steep and becomes steeper as reaction proceeds, indicating dissolution of olivine with little to no precipitation. The slope on the pore side of the LGC histogram becomes shallower, owing to the secondary porosity generation due to the dissolution of olivine.

255 Data from the SGC sample showed that the histograms became uniformly flatter and wider over the duration of the experiment, with an increase in the number of both the darkest and brightest voxels at the expense of the voxels with intermediate grey values (Figure 8). These systematic changes in the absorption behaviour can only be caused by the sample reacting and indeed reflect the dissolution of olivine, the generation of pore space and the precipitation of reaction products, in addition to phase contrast around newly generated edges in the sample. The best fit curves to the histograms evolved systematically during the reaction and intersected in a relatively narrow grey value range (-0.000077, -0.000055) (Figure 87). Voxels with grey values darker than -0.000077 correspond to fluid-filled pores, whose volume proportion increases throughout the reaction process.

3.3 Porosity evolution of LGC compared to SGC

260 Pore space development in LGC is significantly different from SGC. As shown in Figure 5 and 6, the secondary pore space in the LGC developed simultaneously at the interior and the near surface of the sample. However, in the SGC sample, pore space first occurred in area close to the surface and propagated inwards.

265 To further examine the difference in porosity generation of the LGC and SGC sample during the reaction, pore spaces within the subvolumes are segmented from the images and calculated. Figure 8 compares the porosity of subvolume 1 and 2 (Zhu et al., 2016) from SGC and subvolume 3 and 4 from LGC samples. As shown by the figure, initial porosity of the LGC and SGC sample are similar. The rate of porosity increase in the LGC sample is similar to the SGC during the first 36 hours after the reaction started. Porosity of the LGC sample are increasing throughout the duration of the experiment while porosity of the SGC shows a decrease after 90 hours of reaction. In the LGC sample, the porosity increased ~5% and is likely resulted from dissolution. This is consistent with other studies that the precipitate do not occur in olivine carbonation within 36 hours of reaction (e.g. Lisabeth et al., 2017a).

270 We then further evaluated the porosity distribution within the subvolumes by quantifying the porosity of 2D tangential slice along the samples' radial direction. Figure 9 compares the porosity distribution of subvolume 2 from the SGC sample with subvolume 4 from the LGC sample. The subvolume 4 shows a homogeneous increase in porosity of ~5% throughout the entire subvolume. Subvolume 2, while showing an increase of porosity during the first 30 hours of the reaction, starts to show a porosity decrease in areas close to the center of the cup wall after 81 hours of reaction. Comparison of the subvolumes from SGC and LGC revealed that the porosity generation within the LGC sample is relatively homogeneous while the porosity generation within the SGC sample starts to show contrast between the cup's near surface and its interior after 81 hours of reaction. Results from the porosity evaluation further support that the LGC sample is dominated by dissolution with no presence of precipitation.

3.4 Fractures in LGC vs. SGC

280 As discussed in 3.1, the planar fractures observed in the LGC sample are likely a result of the dissolution-assisted extensional crack. This is different from the stretching-induced fractures in SGC (see Zhu et al. 2016) where non-uniform precipitation is indispensable. The dissolution-and-assisted fracturing are in LGC and the stretching-induced fracturing in SGC both observed to generate generated secondary pore space during the experiments, but the dissolution feature fractures in LGC differs distinctively from the reaction induced fractures those on SGC in many ways:

- 285 • Firstly, the dissolution-~~feature~~-assisted fracturing is a single, planar feature in 3-D with no obvious secondary fractures branching out, while the fractures observed in the ~~fine-grained aggregate~~SGC sample formed a network of intersecting cracks. ~~Figure 910a~~ shows the morphology of the dissolution plane and the fracture network in 3D. It's ~~obvious~~shown in Figure 10b that the fractures intersected with each other and formed a complex wedge shape network with the vertex pointing towards the sample's interior. The dissolution-~~feature~~-assisted fracturing mainly developed ~~alone~~along a plane and show less intersection with other features.
 - 290 • Secondly, the LGC sample dominated by dissolution features shows clear evidence for shrinkage of larger grains and disappearance of smaller grains at the interior of the aggregate (Figure 5a). The ~~fine-grained aggregate exhibit~~SGC sample exhibits patches that develop during the reaction which are evidences for the reaction product precipitation- (Zhu et al., 2016).
- 295

- Thirdly, the development of micron-scale dissolution is simultaneous, with the shrinkage of grains occurring both at the surface and the interior of the cup wall (Figure 65 and 9b6a). In contrast, development of the reaction-induced fracturing is successive with most fractures occurred first at the surface and migrated towards the interior of the cup wall. This caused the observed wedge shape of the fracture network (Figure 9a10b). Development of the fractures also exhibits hierarchical sequence with main fractures ~~appeared~~ appearing first. The secondary fractures branch out from the main fracture and divide the sample into smaller ~~patches~~ domains (Figure 72 from Zhu et al., 2016).
- What's more, no precipitates were observed along planar dissolution features in the LGC sample, the cup wall remains straight throughout the experiment. But for the ~~fine-grained aggregate~~ SGC, the cup wall shows clear spalling which is a sign of ~~non~~ non-uniform expansion that links to precipitation in this experiment.

305 3.5 Dissolution and fracturing of individual olivine grain

The reaction affected not only the aggregate but also the individual olivine grains. Both the dissolution ~~feature~~ and ~~reaction-induced~~ fracturing are observed at grain scale- in the SGC sample. Figure 4011 shows a series of image slices through a nanotomography dataset, moving through an olivine grain in the cup wall. The grains clearly exhibit channels (etch pits) in the reaction zone. In video S1 (supplementary materials) it can be seen that these channels penetrate into, and even through olivine grains. As we do not observe any precipitation filling or clogging the tubes, it is therefore reasonable to think that the channels start as etch-pits and grow deeper with the advancing of dissolution and eventually become the through going channels observed here. The tubular shape and the depth of penetration indicate that they are 'worm hole' features, likely resulting from dissolution. The shape and the width of these channels vary, with wider inner channel diameters below the surface suggesting more extensive dissolution at depth. On average, most typical tubes have an inner diameter of around 720nm.

The fracturing is also observed on individual grains at nano-meter scale. Figure 4412 shows nanotomographic evidence for hierarchical fracturing within olivine grains. The secondary fractures developed from the primary fracture and formed in a direction that is perpendicular to the earlier ones.

In the reconstructed microtomographic images of the loose grains from the ~~fine-grained aggregate-cup~~ SGC, we observed the precipitation of secondary minerals on the surface of the olivine grains inside the cup (Figure 4213). On the basis of their rhombohedral shapes we identified these as magnesite crystals. However, the phase contrast between the precipitates and olivine grains is very small, and at the current spatial resolution of ~2 micron, we could not segment precipitates from olivine grain with acceptable uncertainties. Other minerals (e.g. serpentine, brucite, etc., see reaction 1~4) were likely also present in the sample, but could not be isolated at the given image resolution ~~and absorption contrast~~. Measurement of the magnesite circumference revealed continuous growth during the experiment (~~see Figure 5 in Zhu et al., 2016~~) (see Figure 5 in Zhu et al., 2016). The first magnesite crystals emerged after 48 hours, and grains kept nucleating and growing after that. Growth continued until the experiment was aborted and no deceleration could be observed at any point, which indicates that the sample continued reacting. We determined a growth rate for the grain perimeter of $0.772 \mu\text{m}\cdot\text{hour}^{-1}$, which, by assuming cubic shape of the crystal yields an equivalent growth rate of $7.18 \times 10^{-3} \mu\text{m}^3 \cdot \text{hour}^{-1}$. We used a density of $3.01 \text{ g}\cdot\text{cm}^{-3}$ and molar weight of $84.314 \text{ g}\cdot\text{mol}^{-1}$ for magnesite (MgCO_3) in our calculation. Assuming a specific reaction surface of $50 \times 50 \mu\text{m}^2$, this gave a magnesite growth rate of $2.85 \times 10^{-15} \text{ mol}\cdot\text{cm}^{-2}\cdot\text{s}^{-1}$. This is in general in agreement with the calculation of ~~Saldi et al. (2009)~~ Saldi et al. (2009).

The volume change of a loose olivine grain inside the cup was calculated to quantify the competing effect of dissolution and precipitation during olivine carbonation. Individual grains were ~~labeled~~ labelled from the segmented data, and their volumes

335 determined. Figure 4213 plots the volume change of a single grain selected from the loose grains inside the ~~fine-grained~~
~~expSGC~~ over 13 successive microtomographic datasets (covering 146 hours). Magnesite overgrowth causes a significant
roughening of the olivine grain surface. While the volume of the individual magnesite grain steadily increased throughout the
reaction (~~Zhu et al., 2016~~)(Zhu et al., 2016), the total volume of the grain (olivine plus precipitates) fluctuates from time to
340 in grain volume occurred at around 38 hours, which is consistent with a period of vigorous olivine dissolution. The largest
continuous grain volume increase took place between 40 to 70 hours, caused by the precipitation of magnesites. At ~70 hours,
the grain volume again decreased considerably, indicating that dissolution became ~~dominated~~dominant once more. This second
dissolution episode coincides with the appearance of reaction-induced fractures in the aggregate wall at ~68 hours, suggesting
a positive feedback process.

345 4 Discussion

We claim that our experimental observations indicate the activity of two different mechanisms that both create fluid pathways
effectively. These are dissolution-dominated fluid pathway generation at micro-meter scale in the case of the ~~coarse-grained~~
~~aggregateLGC experiment~~ and at nano-meter scale in the case of ~~fine-grained aggregateSGC~~, and reaction-induced fracturing
in the case of the ~~fine-grained aggregateSGC~~. We detail our interpretation in the following sections.

350 4.1 Dissolution and etch-pitting

Dissolution and etch-pitting are important mechanisms that affect the grains' surface morphology and the permeability of the
sample (e.g. ~~King et al., 2010; Røyne and Jamtveit, 2015~~King et al., 2010; Røyne and Jamtveit, 2015). The nanotomographic
observation, that etch-pitting incurs extensive dissolution beneath grain surfaces, was also documented by ~~Lisabeth et al.~~
~~(2017a, 2017b)~~Lisabeth et al. (2017a, 2017b) during the carbonation of dunites. ~~Peuble et al. (2018)~~Peuble et al. (2018) also
355 observed nano-meter scale veinlets forming oblique to sub-vertical channels in partially-carbonated olivine grains during
percolation experiment. The hollowing out of olivines seems especially important in areas where the grain boundary porosity
is decreasing due to the precipitation of secondary minerals. There, subsurface dissolution channels in olivine grains preserve
important fluid pathways and maintain the reaction. This supports the hypothesis of Andreani et al. (2009) that the permeability
can be maintained by the preferential dissolution even in cases where the overall porosity is decreasing. Apart from providing
360 access for fluids, subsurface dissolution features also make the grain more susceptible to fracturing and thereby promote the
generation of fracturing observed in the experiment.

~~The permeability of these dissolution channels was calculated using Hagen-Poiseuille's Law (Poiseuille, 1844)~~The
~~permeability of these dissolution channels was calculated using Hagen-Poiseuille's Law (Poiseuille, 1844)~~ and Darcy's Law
~~(Darcy, 1856)~~(Darcy, 1856). Hagen-Poiseuille's Law allows the calculation of the fluid flow inside a tube in dependency of
365 the pressure gradient:

$$Q = \frac{-\pi r^4 \Delta P}{8\eta \Delta L}, \quad (1)$$

where Q is the volume flow/rate of discharge, r is the radius of the tube, η is the viscosity of the fluid, ΔP is the pressure
difference over the flow length ΔL . Darcy's Law stated that the rate of discharge is proportional to the viscosity of the fluid
and the pressure drop over a given distance, i.e., for a tube with a radius in r:

$$370 \quad Q = \frac{-k\pi r^2 \Delta P}{\eta \Delta L}, \quad (2)$$

where k is the permeability of the tube. Combining the two equations, k can then be derived as:

$$k = \frac{r^2}{8}, \quad (3)$$

In this experiment, r is ~ 6 pixels (360 nm). This yields a permeability of $\sim 1.6 \times 10^{-14} \text{ m}^2$, which is high enough to transmit reacting fluids through these channels. Considering the density of ‘worm hole’ features over the grain, the permeability contributed by the channels could be reduced by two orders of magnitude but is still able to transmit fluid.

380 These intragranular channels contrast the transgranular fractures. But the development of these etch-pitting dissolution channels also provide fluid path for the reaction and allow a more extensive degree of alteration of the grain. They weaken the grains, make them more susceptible to disintegration and provide nucleation sites of the later fracturing. While sparse in our data, we think that over geological time scales the contribution by dissolution channel to bulk permeability and the advance of the reaction would be significant. However, on the time scale of our experiments, these features alone are insufficient to explain the observed self-sustainability of the reaction considering the scale and density of the dissolution channels and we argue that the main contribution must come from volume mismatch cracking in our laboratory study.

4.2 Reaction-induced fracturing

Olivine carbonation could produce up to 44% increase in solid molar volume assuming the reaction can proceed to completion. If such a volume increase takes place, the crystallization pressure generated could be high enough to fracture the host rock (Kelemen et al., 2013; Kelemen and Hirth, 2012)(Kelemen et al., 2013; Kelemen and Hirth, 2012). However, experimental studies on olivine carbonation show no evidence of high crystallization forces (van Noort et al., 2017)(van Noort et al., 2017) but rather suggest that precipitation causes the pore space to fill up and halt the reaction before the crystallization induced pressure reaches the critical value needed to generate fracture (Hövelmann et al., 2012; van Noort et al., 2017).(Hövelmann et al., 2012; van Noort et al., 2017). Our quantitative estimates indicate that in these experiments, ~~crystallization pressure can lead to the~~ maximum $\sim 5\%$ volume expansion, ~~is $\sim 5\%$~~ . This is not enough to break the host rock, as shown in salt crystallization experiments (Scherer, 2004)(Scherer, 2004). Indeed, the nanotomography data show only dissolution features such as etch pits and worm holes, with no evidence of cracks in olivine grains surrounded by precipitates (Figure 4011). The lack of evidence for crystallization pressure-induced cracking is consistent with other experimental studies (e.g. Hövelmann et al., 2012).

~~We interpret our observations from the fine grained aggregate (analyzed in less detail in~~Based on a microtomography experiment, Zhu et al., (2016) ~~as evidence for reaction induced~~proposed an alternative fracturing, ~~and mechanism during olivine carbonation where crystallization pressure is not high enough to directly break the host rock. In their experiment,~~ the observed fracture patterns ~~to form in SGC is~~ analogous to shrinkage cracks (e.g., desiccation cracks; (e.g., Edelman, 1973; Plummer and Gostin, 1981)Edelman, 1973; Plummer and Gostin, 1981). In Zhu et al., (2016)Zhu et al., (2016)’s model, the loose olivine grains inside the cup act as precipitate traps that keep the surface of the cup wall relatively free of precipitation. In the interior of the cup wall though, away from the precipitate traps, the crystallization pressure builds up and causes expansion. While the crystallization pressure is too low to cause shear fracturing of the cup, the expanding cup wall interior stretches the surface of the cup wall and causes it to fail in tension and tear. This is facilitated by the near-constant surface area (which decreases slightly as a result of dissolution). In analogy with desiccation cracks, the resulting fractures form

characteristic and systematic polygonal patterns: The first set of fractures intersect at right angles, and all subsequent fractures divide the sample into smaller polygonal domains with increasing intersection angles. Since the fracture pattern develops successively rather than simultaneously, the higher-order fractures form in a different stress geometry and as a result migrate perpendicular to the surfaces generated by the previous fracturing event.

410 To evaluate the potential of surface stretching as a fracture generating mechanism, we estimated the stress that could be produced by the volume-mismatch in the cup wall of SGC. We did so by identifying and tracking grains whose spatial coordinates (x, y, z) changed continually as the sample expanded. ~~Measurements of the distance~~ Distances between these grains were measured at different times. Our measurements indicate an average expansion of ~9.1 μm over a distance of ~260 μm from 7 hours to 125.9 hours after the start of the experiment. The results revealed an axial elongation of 2.78~4.71% in
415 ~120 hours in the LGC sample. However, little to no expansion was observed at the near surface of the sample's cup wall. This would translate into an axial strain of ~0.03 of the outer layer in order to compensate the volume mismatch. The elastic moduli and strengths of the synthesized porous olivine aggregates are similar to weak sandstones. Using a Young's modulus of ~10 GPa yields extensional stresses generated due to the expansion of ~300 MPa, easily exceeding the tensile strength of the sample (~10MPa). Interestingly, our estimate of extensional stress generated by the volume mismatch is of the same
420 magnitude to the stress from crystallization pressurization (e.g. ~~Kelemen et al., 2013~~ Kelemen et al., 2013). For natural peridotite, Young's moduli range from 108 to 194 GPa (~~Christensen, 1966~~ Christensen, 1966), tensile strength is 50 to 290 MPa and spall strength is ~58 MPa (~~He et al., 1996~~ He et al., 1996). An equivalent volume expansion of ~10% in nature could lead to a stress of 3.24 GPa. In both cases, the stress is more than sufficient to fracture the material. However, these are simple estimations of stress and strain made with basic assumptions and local conditions. Considering the extent of the local
425 carbonation reaction and how the expansion in the center is affecting straining of the outer layers, the estimated stress can be considerably lower but should still be in a range that is sufficient to break the material.

To generate the expansion cracks via surface stretching, the volume mismatch must be substantial, which requires to keep the near surface region free of precipitates. Zhu et al. (2016) suggested that the loose olivine grains inside the sample cup worked as precipitate traps/attractors in this experiment. Because the rate of crystal growth decreases drastically as the curvature of
430 the substrate increases (García et al., 2013; Ziese et al., 2013), large grains in general are preferred sites for precipitation of new crystals. With a size contrast of ~2 orders magnitude, the loose olivine grains (100-500 μm) in the immediate vicinity of the inner cup surface fulfilled the function of precipitate traps and thereby kept precipitation level at the surface of the olivine cup wall low.

We tested the idea of volume mismatch cracking by conducting the LGC experiment. Now the size contrast between the grains
435 forming the aggregate in the cup wall and the loose grains inside the cup was significantly reduced, and we expected less efficient precipitate trapping, and consequently little to no reaction-induced cracks. The experimental results support this idea. The only planar features observed in the new microtomography experiment are planar dissolution ~~features~~ assisted cracking (Figure 6 and 10a).

A detailed examination of the dissolution channel shown in Fig. 6 revealed no evidence of precipitates there. This places doubt
440 on the crystallization pressure being responsible for fracturing during olivine carbonation. If not, what could be an alternative explanation for the observed fracturing? To further address this question, we examined the porosity evolution and distribution in the 3-D tomographic datasets.

Despite the histogram analysis revealed a bulk increase in the porosity of the cup wall during the experiment, the distribution of these newly generated pores was inhomogeneous in the sample (Figure ~~139~~ and 14). This perturbed the initially

445 homogeneous porosity distribution. This effect became particularly apparent in subvolume 2, which started to exhibit higher
porosity where it was closest to the outer surface of the sample after 68 hours (see Video S2, S3, S4 for details). The difference
in porosity distribution within the sample became more pronounced as the reaction proceeded, with porosity in the outer surface
of the cup wall increasing while the porosity inside the cup decreased. In our interpretation, this change in the pore volume
450 reflects a contrast in the precipitation rate where precipitation proceeded more slowly in the outer part compared to the inner
part of the sample wall, leading to different rates of expansion and the generation of tensile stresses.

The ‘expansion cracks via stretching’ mechanism can explain the observed microstructure evolution in two subvolumes of
SGC (Figure 4). Since subvolume 2 is located at the periphery of the cup, it would be fractured before subvolume 1 which
locates in the center of the cup wall. This predict from the ‘expansion cracks via stretching’ is consistent with the observed
distribution of pore space that most porous area locates close to the periphery. This mechanism also explains why the fractures
455 tend to develop perpendicular to the reaction surfaces. Similar models relating the reaction generated stress and fractures has
also been used to explain other exfoliation cracks (e.g. Blackwelder, 1925Blackwelder, 1925).

In summary, two fundamental observations from our experiments are inconsistent with the “~~internal cracks generated by~~
crystallization pressure”-mechanism induced fracturing” model and form strong arguments against ~~the existence of any~~
significanthigh crystallization forces (i.e., sufficient to break the surrounding rock) (Figure ~~40, 13~~11, 14). Firstly, if the cracks
460 were generated directly by crystallization pressure, we should expect them to initiate in region with intense precipitation and
porosity reduction. However, in the outer layer of our sample where the fractures are observed, no precipitates formed prior to
the fracturing. Secondly, on the nanoscale, the channels formed by dissolution show hollow and smooth inner surfaces and no
precipitation of magnesite (or any other minerals) which shows evidences of low crystallization pressure.

Our detailed analyses provide quantitative support to the “surface cracking via volume mismatch” model first proposed by
465 ~~Zhu et al. (2016)~~Zhu et al. (2016). Previous experimental studies on olivine carbonation show that the crystallization force is
low (~~van Noort et al., 2017~~)(van Noort et al., 2017), suggesting that breaking host rocks by crystallization pressure as in salt
crystallization is unlikely which is in contrast with fracture networks that are commonly observed in naturally occurred
serpentinized and carbonated peridotites (Iyer et al., 2008; Macdonald and Fyfe, 1985). We present a resolution to this
conundrum by documenting a process that allows fracturing without a high crystallization force.

470 **4.3 Coupled-mechanisms of dissolution and precipitation-driven fracturing**

The findings of this study can be summarized in a mechanism that couples dissolution and precipitation during olivine
carbonation. If dissolution and precipitation are heterogeneously distributed in a rock, non-uniform volume expansion can
cause breaking of the host rock via surface stretching. In nature, heterogeneity in the porosity and permeability of a rock
formation is common, which may cause non-uniform concentration of reaction and distribution of precipitation (Wells et al.,
475 2017). As shown in our study, the resulting volume mismatch could lead to expansion fractures. The fractures provide new
fluid pathways and expose fresh reactive surfaces to sustain the carbonation. In a long-term, fluid pathways may be provided
by “worm-hole” etch pitting. Dissolution channels could deteriorate rock strength over longer time scales (Figure 4415).

In a field study on serpentinization of peridotites at ocean ridges, Rouméjon and Cannat (2014) show that the reaction-induced
fracturing occurs in the early stages of serpentinization (probably before 20% of serpentinization) while the rest of the volume
480 increase is accommodated by the serpentine itself and dissolution processes dominate until completion of the reaction. Clearly,
natural processes are more complex. Laboratory studies are not capable of simulating nature settings due to the vastly different
length and time scale. Instead, we focus on understanding the underlying mechanism of porosity generation during olivine

485 carbonation reaction. Using the coupled dissolution and fracturing model described above, we postulate that at the beginning of a carbonation reaction, dissolution plays an important role in maintaining porosity. As reaction progresses, no-uniform expansion of the rock due to precipitation could lead to fractures. Once the host rock is fractured, accelerated reaction takes place to achieve 100% carbonation.

In general, several different mechanisms seem to facilitate olivine ~~alteration~~carbonation and contribute to sustaining it. On relatively short time scales, rapid reaction-induced tensile fracturing could be the dominating mechanism that maintains the reaction, whereas on a longer timescale, dissolution and the formation of channel-like structures may dominate.

490 **5 Conclusions**

Using synchrotron-based micro- and nano-tomography, we documented and quantified the reaction progress during olivine-fluid interaction on the micron scale. This allowed us to identify mechanism that sustain the reaction despite its large positive volume change.

In summary, our experiment results suggest:

- 495 • The reaction-induced fracturing observed in our experiments results from non-uniform volume expansion. Tensile stresses arise from heterogeneous precipitation and the resulting contrast in the expansion: between a faster expanding interior and a slower expanding near-surface.
- 500 • Even though the dissolution cannot be used alone to explain the sustainability of the experimental-time-scale olivine carbonation, it provides evidence that dissolution etch-pits can provide fluid path and fresh reaction surface for the reaction to proceed. This helps in explaining the naturally occurring complete alteration of peridotite, as the time scale for natural carbonation ranges from thousands to million years. Even if the dissolution channelizing would only allow slow fluid flow, it could still induce significant alteration given time.
- 505 • The coupled-mechanism of dissolution and reaction-induced fracturing accounts for maintaining the reaction processes during olivine carbonation. It explains on different time and space scale about the formation of observed natural outcrops of completely carbonated peridotite.
- The results from our experimental study also provide new insights into the application of CO₂ mineral sequestration.

References

- 510 Andreani, M., Luquot, L., Gouze, P., Godard, M., Hoise, E. and Gibert, B.: Experimental Study of Carbon Sequestration Reactions Controlled by the Percolation of CO₂-Rich Brine through Peridotites, *Environ. Sci. Technol.*, 43(4), 1226–1231, doi:10.1021/es8018429, 2009.
- Bedford, J., Fousseis, F., Leclère, H., Wheeler, J. and Faulkner, D.: A 4D view on the evolution of metamorphic dehydration reactions, *Sci. Rep.*, 7(1), doi:10.1038/s41598-017-07160-5, 2017.
- Beinlich, A. and Austrheim, H.: In situ sequestration of atmospheric CO₂ at low temperature and surface cracking of serpentinized peridotite in mine shafts, *Chem. Geol.*, 332–333, 32–44, doi:10.1016/j.chemgeo.2012.09.015, 2012.
- 515 Beinlich, A., Plümper, O., Hövelmann, J., Austrheim, H. and Jamtveit, B.: Massive serpentinite carbonation at Linnajavri, N-Norway, *Terra Nov.*, 24(6), 446–455, doi:10.1111/j.1365-3121.2012.01083.x, 2012.
- Blackwelder, E.: Exfoliation as a Phase of Rock Weathering, *J. Geol.*, 33(8), 793–806, 1925.

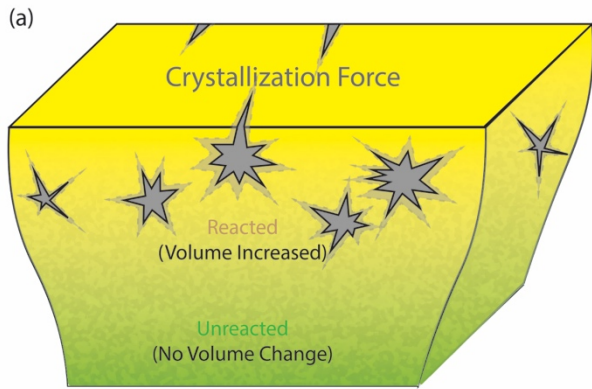
- Christensen, N. I.: Elasticity of Ultrabasic Rocks, *J. Geophys. Res.*, 71(24), 5921–5931, doi:10.1029/JZ071i024p05921, 1966.
- 520 Cloetens, P., Barrett, R., Baruchel, J., Guigay, J. P. and Schlenker, M.: Phase objects in synchrotron radiation hard x-ray imaging, *J. Phys. D. Appl. Phys.*, 29(1), 133–146, doi:10.1088/0022-3727/29/1/023, 1996.
- Darcy, H.: Les fontaines publiques de la ville de Dijon, Recherche, 647 [online] Available from: <http://scholar.google.com/scholar?hl=en&btnG=Search&q=intitle:Les+fontaines+publiques+de+la+ville+de+dijon#0>, 1856.
- Deschamps, F., Godard, M., Guillot, S. and Hattori, K.: Geochemistry of subduction zone serpentinites: A review, *Lithos*, 178, 96–127, doi:10.1016/j.lithos.2013.05.019, 2013.
- 525 Eberhardt, E., Stimpson, B. and Stead, D.: Effects of Grain Size on the Initiation and Propagation Thresholds of Stress-induced Brittle Fractures, *Rock Mech. Rock Eng.*, 32(2), 81–99, doi:10.1007/s006030050026, 1999.
- Edelman, N.: Tension cracks parallel with the axial plane, 1973.
- Emmanuel, S. and Berkowitz, B.: Suppression and stimulation of seafloor hydrothermal convection by exothermic mineral hydration, *Earth Planet. Sci. Lett.*, 243(3–4), 657–668, doi:10.1016/j.epsl.2006.01.028, 2006.
- 530 Escartín, J., Hirth, G. and Evans, B.: Effects of serpentinitization on the lithospheric strength and the style of normal faulting at slow-spreading ridges, *Earth Planet. Sci. Lett.*, 151(3–4), 181–189, doi:10.1016/S0012-821X(97)81847-X, 1997.
- Evans, B. W.: Metamorphism of alpine peridotite and serpentinite, *Annu. Rev. Earth Planet. Sci.*, 5, 397–447, doi:10.1146/annurev.ea.05.050177.002145, 1977.
- 535 Falk, E. S. and Kelemen, P. B.: Geochemistry and petrology of listvenite in the Samail ophiolite, Sultanate of Oman: Complete carbonation of peridotite during ophiolite emplacement, *Geochim. Cosmochim. Acta*, 160, 70–90, doi:10.1016/j.gca.2015.03.014, 2015.
- Fryer, P., Mottl, M., Johnson, L., Haggerty, J., Phipps, S. and Maekawa, H.: Serpentine bodies in the forearcs of western pacific convergent margins: Origin and associated fluids, in *Geophysical Monograph Series*, vol. 88, pp. 259–279., 1995.
- 540 Fusses, F., Schrank, C., Liu, J., Karrech, A., Llana-Fúnez, S., Xiao, X. and Regenauer-Lieb, K.: Pore formation during dehydration of a polycrystalline gypsum sample observed and quantified in a time-series synchrotron X-ray micro-tomography experiment, *Solid Earth*, 3(1), 71–86, doi:10.5194/se-3-71-2012, 2012.
- Fusses, F., Xiao, X., Schrank, C. and De Carlo, F.: A brief guide to synchrotron radiation-based microtomography in (structural) geology and rock mechanics, *J. Struct. Geol.*, 65, 1–16, doi:10.1016/j.jsg.2014.02.005, 2014a.
- 545 Fusses, F., Steeb, H., Xiao, X., Zhu, W. L., Butler, I. B., Elphick, S. and Mäder, U.: A low-cost X-ray-transparent experimental cell for synchrotron-based X-ray microtomography studies under geological reservoir conditions, *J. Synchrotron Radiat.*, 21(1), 251–253, doi:10.1107/S1600577513026969, 2014b.
- García, N. A., Register, R. A., Vega, D. A. and Gómez, L. R.: Crystallization dynamics on curved surfaces, *Phys. Rev. E - Stat. Nonlinear, Soft Matter Phys.*, 88(1), doi:10.1103/PhysRevE.88.012306, 2013.
- 550 Gislason, S. R., Wolff-Boenisch, D., Stefansson, A., Oelkers, E. H., Gunnlaugsson, E., Sigurdardottir, H., Sigfusson, B., Broecker, W. S., Matter, J. M. and Stute, M.: Mineral sequestration of carbon dioxide in basalt: A pre-injection overview of the CarbFix project, *Int. J. Greenh. Gas Control*, 4(3), 537–545, doi:10.1016/j.ijggc.2009.11.013, 2010.
- Goff, F. and Lackner, K. S.: Carbon dioxide sequestering using ultramafic rocks, *Environ. Geosci.*, 5(3), 89 LP-101, doi:10.1046/j.1526-0984.1998.08014.x, 1998.
- 555 Grandstaff, D. E.: Changes in surface area and morphology and the mechanism of forsterite dissolution, *Geochim. Cosmochim. Acta*, 42(12), 1899–1901, doi:10.1016/0016-7037(78)90245-4, 1978.
- Gürsoy, D., De Carlo, F., Xiao, X. and Jacobsen, C.: TomoPy: A framework for the analysis of synchrotron tomographic data, *J. Synchrotron Radiat.*, 21(5), 1188–1193, doi:10.1107/S1600577514013939, 2014.

- Hansen, L. D., Dipple, G. M., Gordon, T. M. and Kellett, D. A.: Carbonated serpentinite (listwanite) at Atlin, British Columbia: A geological analogue to carbon dioxide sequestration, *Can. Mineral.*, 43(1), 225–239, doi:10.2113/gscanmin.43.1.225, 2005.
- 560 He, H., Jin, X., Jing, F. and Ahrens, T. J.: Characteristic of dynamic tensile fracture in augite-peridotite, in *AIP Conference Proceedings*, vol. 370, pp. 593–596, AIP., 1996.
- Heilbronner, R. and Barrett, S.: *Image Analysis in Earth Sciences*, Springer Berlin Heidelberg, Berlin, Heidelberg., 2014.
- Hövelmann, J., Austrheim, H. and Jamtveit, B.: Microstructure and porosity evolution during experimental carbonation of a natural peridotite, *Chem. Geol.*, 334, 254–265, doi:10.1016/j.chemgeo.2012.10.025, 2012.
- 565 Iyer, K., Jamtveit, B., Mathiesen, J., Malthe-Sørenssen, A. and Feder, J.: Reaction-assisted hierarchical fracturing during serpentinitization, *Earth Planet. Sci. Lett.*, 267(3–4), 503–516, doi:10.1016/j.epsl.2007.11.060, 2008.
- Jamtveit, B., Putnis, C. V. and Malthe-Sørenssen, A.: Reaction induced fracturing during replacement processes, *Contrib. to Mineral. Petrol.*, 157(1), 127–133, doi:10.1007/s00410-008-0324-y, 2009.
- Jamtveit, B., Kobchenko, M., Austrheim, H., Malthe-Sørenssen, A., Røyne, A. and Svensen, H.: Porosity evolution and crystallization-driven fragmentation during weathering of andesite, *J. Geophys. Res. Solid Earth*, 116(12), 1–12, doi:10.1029/2011JB008649, 2011.
- 570 Johannes, W.: An experimental investigation of the system MgO-SiO₂-H₂O-CO₂, *Am. J. Sci.*, 267(9), 1083–1104, doi:10.2475/ajs.267.9.1083, 1969.
- Kaestner, A., Lehmann, E. and Stampanoni, M.: Imaging and image processing in porous media research, *Adv. Water Resour.*, 31(9), 1174–1187, doi:10.1016/j.advwatres.2008.01.022, 2008.
- 575 Kelemen, P. B. and Hirth, G.: Reaction-driven cracking during retrograde metamorphism: Olivine hydration and carbonation, *Earth Planet. Sci. Lett.*, 345–348, 81–89, doi:10.1016/j.epsl.2012.06.018, 2012.
- Kelemen, P. B. and Matter, J. M.: In situ carbonation of peridotite for CO₂ storage, *Proc. Natl. Acad. Sci. U. S. A.*, 105(45), 17295–17300, doi:10.1073/pnas.0805794105, 2008.
- 580 Kelemen, P. B., Matter, J., Streit, E. E., Rudge, J. F., Curry, W. B. and Blusztajn, J.: Rates and Mechanisms of Mineral Carbonation in Peridotite: Natural Processes and Recipes for Enhanced, in situ CO₂ Capture and Storage, *Annu. Rev. Earth Planet. Sci.*, 39(1), 545–576, doi:10.1146/annurev-earth-092010-152509, 2011.
- Kelemen, P. B., Savage, H. and Hirth, G.: Reaction-Driven Cracking During Mineral Hydration, Carbonation and Oxidation, in *Poromechanics V*, vol. c, pp. 823–826, American Society of Civil Engineers, Reston, VA., 2013.
- 585 King, H. E., Plümper, O. and Putnis, A.: Effect of Secondary Phase Formation on the Carbonation of Olivine, *Environ. Sci. Technol.*, 44(16), 6503–6509, doi:10.1021/es9038193, 2010.
- Lisabeth, H., Zhu, W., Xing, T. and De Andrade, V.: Dissolution-Assisted Pattern Formation During Olivine Carbonation, *Geophys. Res. Lett.*, 44(19), 9622–9631, doi:10.1002/2017GL074393, 2017a.
- Lisabeth, H. P., Zhu, W., Kelemen, P. B. and Ilgen, A.: Experimental evidence for chemo-mechanical coupling during carbon mineralization in ultramafic rocks, *Earth Planet. Sci. Lett.*, 474, 355–367, doi:10.1016/j.epsl.2017.06.045, 2017b.
- 590 Macdonald, A. H. and Fyfe, W. S.: Rate of serpentinitization in seafloor environments, *Tectonophysics*, 116(1–2), 123–135, doi:10.1016/0040-1951(85)90225-2, 1985.
- Mani, D., Nirmal Charan, S. and Kumar, B.: Assessment of carbon dioxide sequestration potential of ultramafic rocks in the greenstone belts of southern India, *Curr. Sci.*, 94(1), 53–60, 2008.
- 595 Moore, D. E., Lockner, D. A., Summers, R., Ma, S. and Byerlee, J. D.: Strength of crisolite-serpentinite gouge under hydrothermal conditions: Can it explain a weak San Andreas fault?, *Geology*, 24(11), 1041–1044, doi:10.1130/0091-7613(1996)024<1041, 1996.

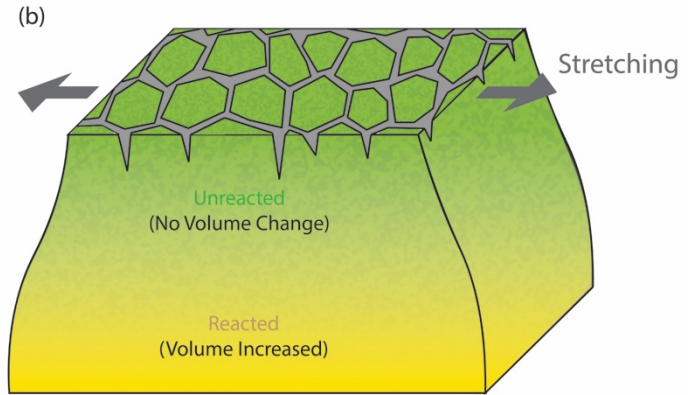
- 600 Nasir, S., Al Sayigh, A. R., Al Harthy, A., Al-Khribash, S., Al-Jaaidi, O., Musllam, A., Al-Mishwat, A. and Al-Bu'saidi, S.: Mineralogical and geochemical characterization of listwaenite from the Semail Ophiolite, Oman, *Chemie der Erde - Geochemistry*, 67(3), 213–228, doi:10.1016/j.chemer.2005.01.003, 2007.
- van Noort, R., Wolterbeek, T., Drury, M., Kandianis, M. and Spiers, C.: The Force of Crystallization and Fracture Propagation during In-Situ Carbonation of Peridotite, *Minerals*, 7(10), 190, doi:10.3390/min7100190, 2017.
- Peuble, S., Andreani, M., Gouze, P., Pollet-Villard, M., Reynard, B. and Van de Moortele, B.: Multi-scale characterization of the incipient carbonation of peridotite, *Chem. Geol.*, 476, 150–160, doi:10.1016/j.chemgeo.2017.11.013, 2018.
- 605 Plummer, P. S. and Gostin, V. a: Shrinkage cracks: desiccation or synaeresis?, *J. Sediment. Petrol.*, 51(4), 1147–1156, doi:10.1306/212F7E4B-2B24-11D7-8648000102C1865D, 1981.
- Poiseuille, J. L. M.: Recherches experimentales sur le mouvement des liquides dans les tubes de tres petits diametres, Imprimerie Royale. [online] Available from: <https://www.irphe.fr/~clanet/otherpaperfile/articles/Poiseuille/%0Ahttps://www.irphe.fr/~clanet/otherpaperfile/articles/Poiseuille/poiseuille1840a.pdf>, 1844.
- 610 Poiseuille, J. L. M.: Recherches experimentales sur le mouvement des liquides dans les tubes de tres petits diametres, Imprimerie Royale. [online] Available from: <https://www.irphe.fr/~clanet/otherpaperfile/articles/Poiseuille/%0Ahttps://www.irphe.fr/~clanet/otherpaperfile/articles/Poiseuille/poiseuille1840a.pdf>, 1844.
- Power, I. M., Harrison, A. L., Dipple, G. M., Wilson, S. A., Kelemen, P. B., Hitch, M. and Southam, G.: Carbon Mineralization: From Natural Analogues to Engineered Systems, *Rev. Mineral. Geochemistry*, 77(1), 305–360, doi:10.2138/rmg.2013.77.9, 2013.
- 615 Rouméjon, S. and Cannat, M.: Serpentinization of mantle-derived peridotites at mid-ocean ridges: Mesh texture development in the context of tectonic exhumation, *Geochemistry, Geophys. Geosystems*, 15(6), 2354–2379, doi:10.1002/2013GC005148, 2014.
- Røyne, A. and Jamtveit, B.: Pore-Scale Controls on Reaction-Driven Fracturing, *Rev. Mineral. Geochemistry*, 80(1), 25–44, doi:10.2138/rmg.2015.80.02, 2015.
- 620 Rudge, J. F., Kelemen, P. B. and Spiegelman, M.: A simple model of reaction-induced cracking applied to serpentinization and carbonation of peridotite, *Earth Planet. Sci. Lett.*, 291(1–4), 215–227, doi:10.1016/j.epsl.2010.01.016, 2010.
- Saldi, G. D., Jordan, G., Schott, J. and Oelkers, E. H.: Magnesite growth rates as a function of temperature and saturation state, *Geochim. Cosmochim. Acta*, 73(19), 5646–5657, doi:10.1016/j.gca.2009.06.035, 2009.
- Scherer, G. W.: Stress from crystallization of salt, *Cem. Concr. Res.*, 34(9), 1613–1624, doi:10.1016/j.cemconres.2003.12.034, 2004.
- 625 Singh, S. K.: Relationship among fatigue strength, mean grain size and compressive strength of a rock, *Rock Mech. Rock Eng.*, 21(4), 271–276, doi:10.1007/BF01020280, 1988.
- Ulven, O. I., Storheim, H., Austrheim, H. and Malthe-Sørenssen, A.: Fracture initiation during volume increasing reactions in rocks and applications for CO₂ sequestration, *Earth Planet. Sci. Lett.*, 389, 132–142, doi:10.1016/j.epsl.2013.12.039, 2014.
- 630 Velbel, M. A.: Dissolution of olivine during natural weathering, *Geochim. Cosmochim. Acta*, 73(20), 6098–6113, doi:10.1016/j.gca.2009.07.024, 2009.
- Velbel, M. A. and Ranck, J. M.: Etch pits on naturally altered olivine from dunites of the Appalachian Blue Ridge Mountains, North Carolina, USA, *Mineral. Mag.*, 72(1), 145–148, doi:10.1180/minmag.2008.072.1.145, 2008.
- 635 Wells, R. K., Xiong, W., Sesti, E., Cui, J., Giammar, D., Skemer, P., Hayes, S. E. and Conradi, M. S.: Spatially-variable carbonation reactions in polycrystalline olivine, *Geochim. Cosmochim. Acta*, 204, 252–266, doi:10.1016/j.gca.2017.02.003, 2017.
- Weyl, P. K.: Pressure solution and the force of crystallization: a phenomenological theory, *J. Geophys. Res.*, 64(11), 2001–2025, doi:10.1029/JZ064i011p02001, 1959.
- Wilson, M. J.: Weathering of the primary rock-forming minerals: processes, products and rates, *Clay Miner.*, 39(3), 233–266, doi:10.1180/0009855043930133, 2004.

- 640 Wilson, M. J. and Jones, D.: Lichen weathering of minerals: implications for pedogenesis, *Geol. Soc. London, Spec. Publ.*, 11(1), 5–12, doi:10.1144/GSL.SP.1983.011.01.01, 1983.
- Winkler, E. M. and Singer, P. C.: Crystallization pressure of salts in stone and concrete, *Bull. Geol. Soc. Am.*, 83(11), 3509–3514, doi:10.1130/0016-7606(1972)83[3509:CPOISS]2.0.CO;2, 1972.
- 645 Zhu, W., Montesi, L. G. J. and Wong, T. F.: Shear-enhanced compaction and permeability reduction: Triaxial extension tests on porous sandstone, *Mech. Mater.*, 25(3), 199–214, doi:10.1016/S0167-6636(97)00011-2, 1997.
- Zhu, W., Fousseis, F., Lisabeth, H. P., Xing, T., Xiao, X., De Andrade, V. and Karato, S. I.: Experimental evidence of reaction-induced fracturing during olivine carbonation, *Geophys. Res. Lett.*, 43(18), 9535–9543, doi:10.1002/2016GL070834, 2016.
- Ziese, F., Maret, G. and Gasser, U.: Heterogeneous nucleation and crystal growth on curved surfaces observed by real-space imaging, *J. Phys. Condens. Matter*, 25(37), doi:10.1088/0953-8984/25/37/375105, 2013.

650



Crystallization Pressurization Induced Fracturing



Stretching Induced Fracturing

655 Figure 1: Illustration of the mechanisms of reaction-induced fracturing during olivine-fluid interaction. a) The crystallization pressurization ~~described model describes~~ the development of fractures caused by crystallization forces exerted on the surroundings due to growth of precipitates. Salt crystallization (Scherer, 2004)(Scherer, 2004) is a typical example of the crystallization pressure induced fracturing. The fractures first appear at areas where precipitation is most concentrated and propagate outwards. b) The surface cracking model describes the development of fractures as a result of a contrast in expansion which causes stretching at the surface. A difference in the precipitation rate between the periphery and interior of the sample causes them to expand in different rates with the insideinterior expanding faster than the outsidesurface. This builds up the tensile stress at the surface that fractures the sample and leads to a development of a polygonal fracture network. The fractures propagate from the surface towards the insideinwards.

660

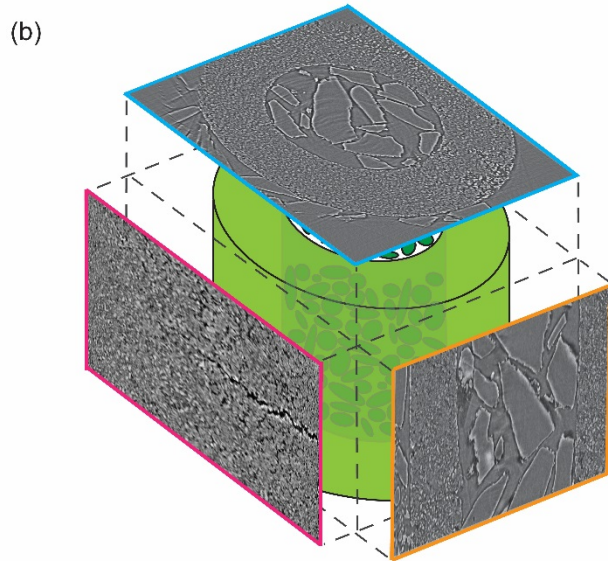
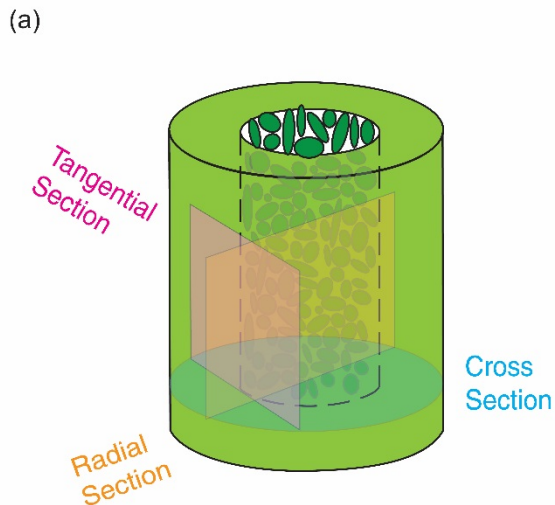


Figure 2: Illustration of sample configuration. a) The sample is composed a sintered olivine aggregate cup with loose olivine sand fillings (grain size 100-500 μm). Quantitative microtomographic analyses are conducted on the tangential (pink), radial (orange) and cross (blue) section of the sample. b) Example of the tomographic images that was used in the 2D examination of Zhu et al. (2016).

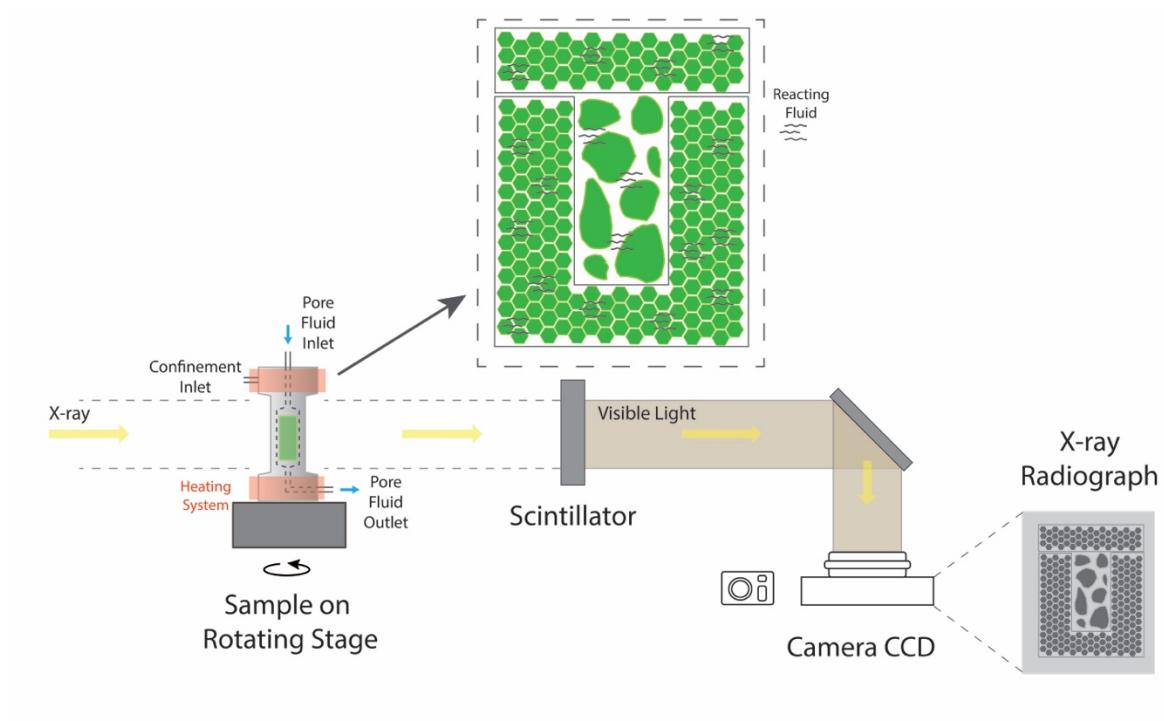
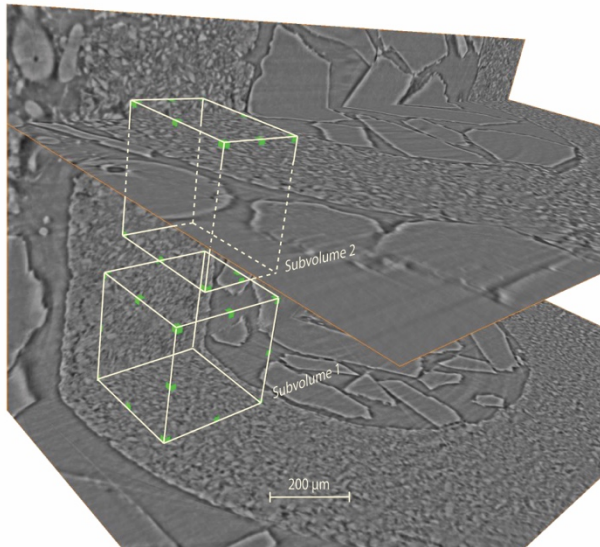


Figure 3: Experimental setup for dynamic microtomography. Inside the x-ray transparent pressure cell, the confining pressure, pore pressure and temperature can be controlled independently. The synchrotron radiation imaging records radiographs of the sample at in-situ conditions with ongoing reaction at different angular positions with the sample being rotated.

(a) SGC



(b) LGC

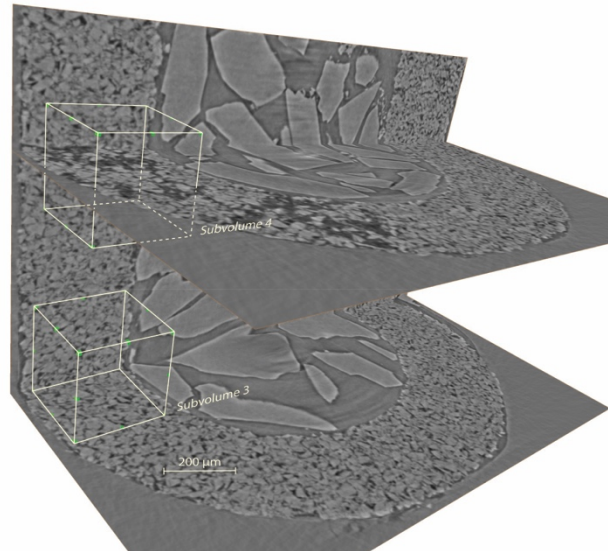
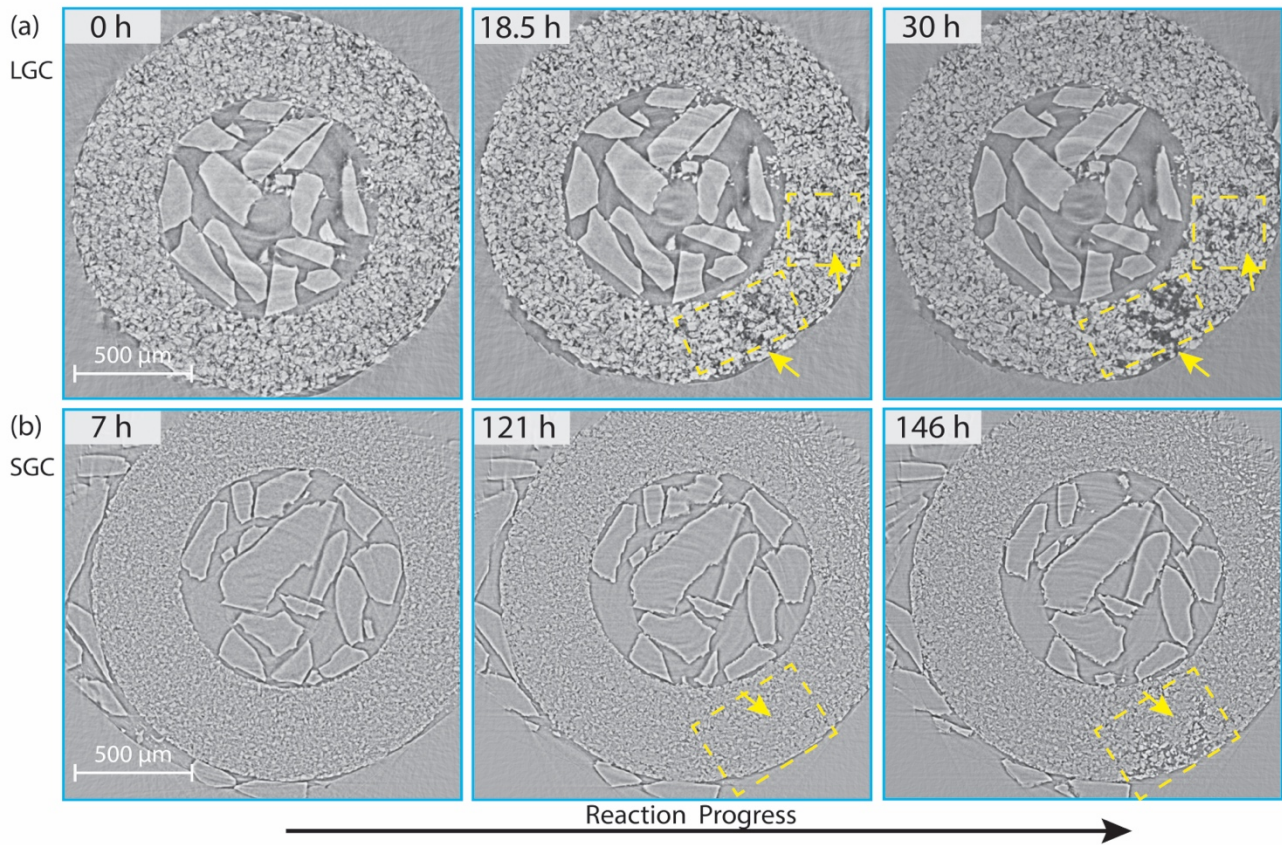
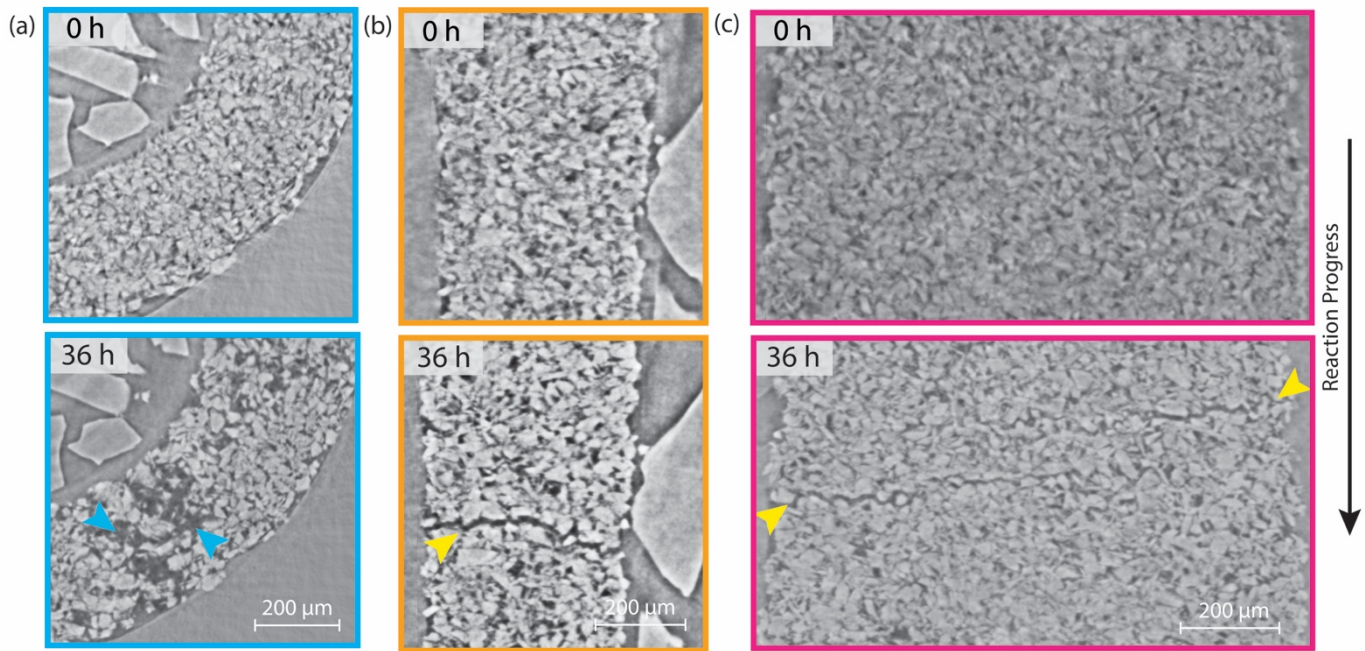


Figure 4: ~~The sub-region of the fine-grained aggregate sample examined in detail.~~ Positions of the ~~two~~ subvolumes in the cup wall. ~~Subvolume of a) SGC and b) LGC, where quantitative 3D microstructure analyses were performed.~~ In the SGC sample, subvolume 1 (bottom box) is located at the center of the cup wall. Subvolume 2 (top box) is located adjacent to the outer rim of the wall. In the LGC sample, both subvolume 3 (bottom box) and subvolume 4 (top box) are located at the center of the cup wall.



680 **Figure 5: Reconstructed images showing horizontal cross section view of the sample undergoing olivine carbonation. a) Coarse-grained aggregates exhibit In the LGC sample, original olivine grains shrink, and secondary pore space appears (yellow arrows), suggesting dissolution features in which grain of olivine shrank and formed secondary pore spaces. Most of the large pore spaces concentrate at the interior of the cup wall (highlighted by yellow dash lines). b) Fine-grained aggregates show that In the SGC sample, the fractures first developed at the surface of the cup and propagated from the outer rim into the cup wall (highlighted by yellow dash lines). Larger pore space distributes mainly near the rim.**



685

Figure 6: a) Dissolution feature in the cross-sectional images of the LGC sample. 3D examination reveals that these dissolution features (blue arrowheads) are associated with planar fractures (yellow arrowheads) appeared in b) the radial and c) the tangential section images. The boarder color of each section corresponds to color code given in Figure 2.

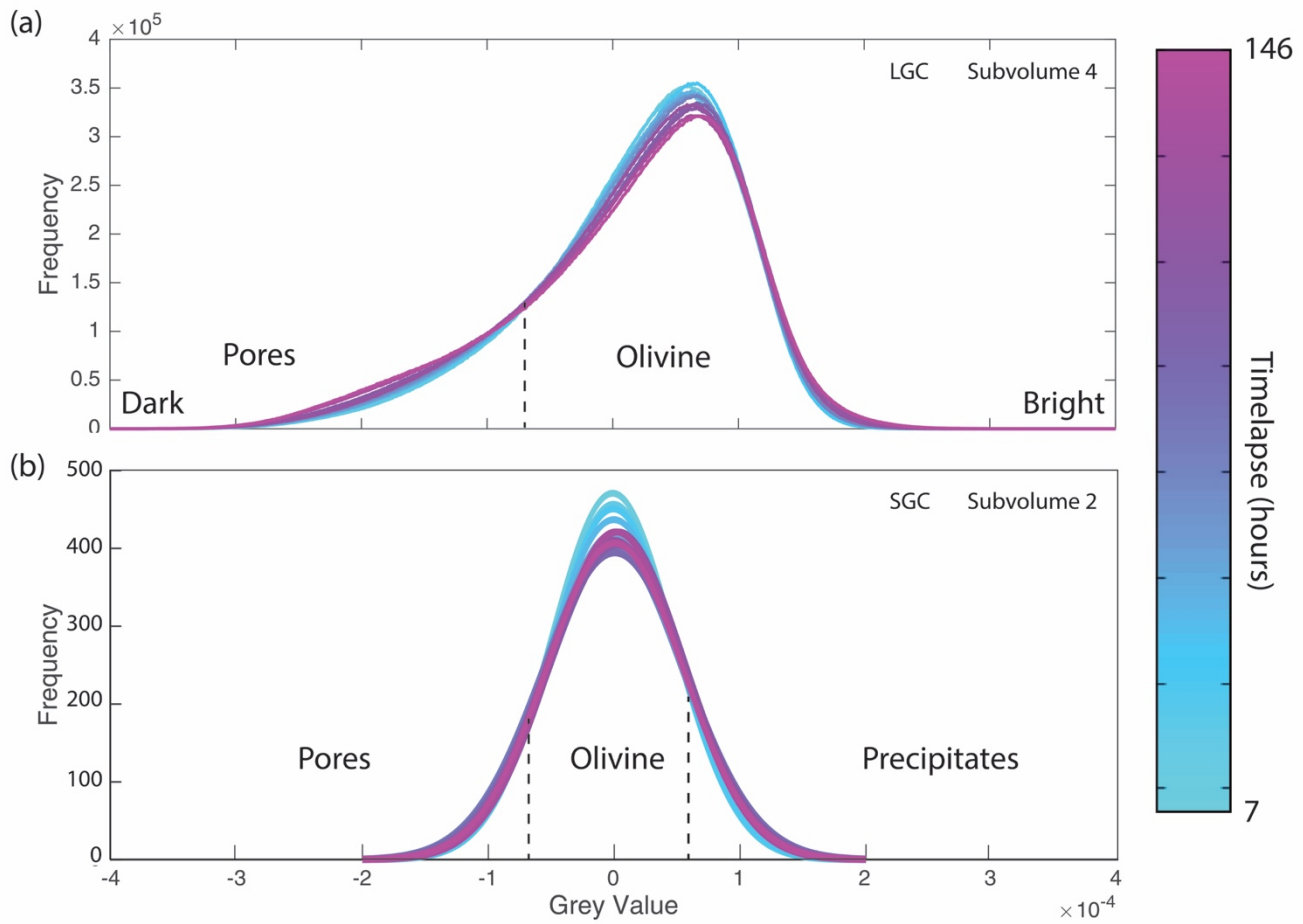


Figure 7: Best-fits for the grey value distribution histograms of the sample at different stages of the reaction. in a) subvolume 4 from LGC sample and b) subvolume 2 from SGC sample. Different colors represent time lapses as shown. Pores, olivine, and precipitates are identified based on their grey value ranges. Higher values correspond to lighter grey (solids). The more negative a value is, the darker the grey color becomes (e.g., pores are black). b) Segmentation of pore space in subvolume 1 (at 146 hours). In the 2D cross-sectional images (marked as planes x, y, z), the red areas represent segmented pore spaces. Histograms of SCG sample were calculated from a 2D image (Zhu et al., 2016), whereas the histograms of LGC sample were calculated from 3D datasets.

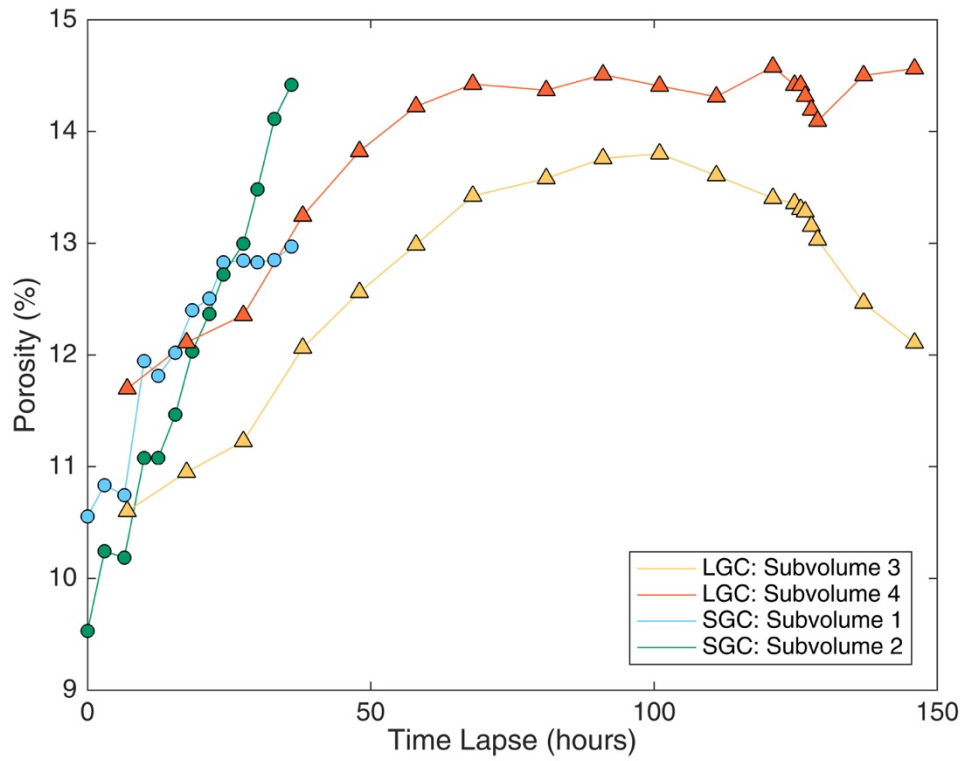
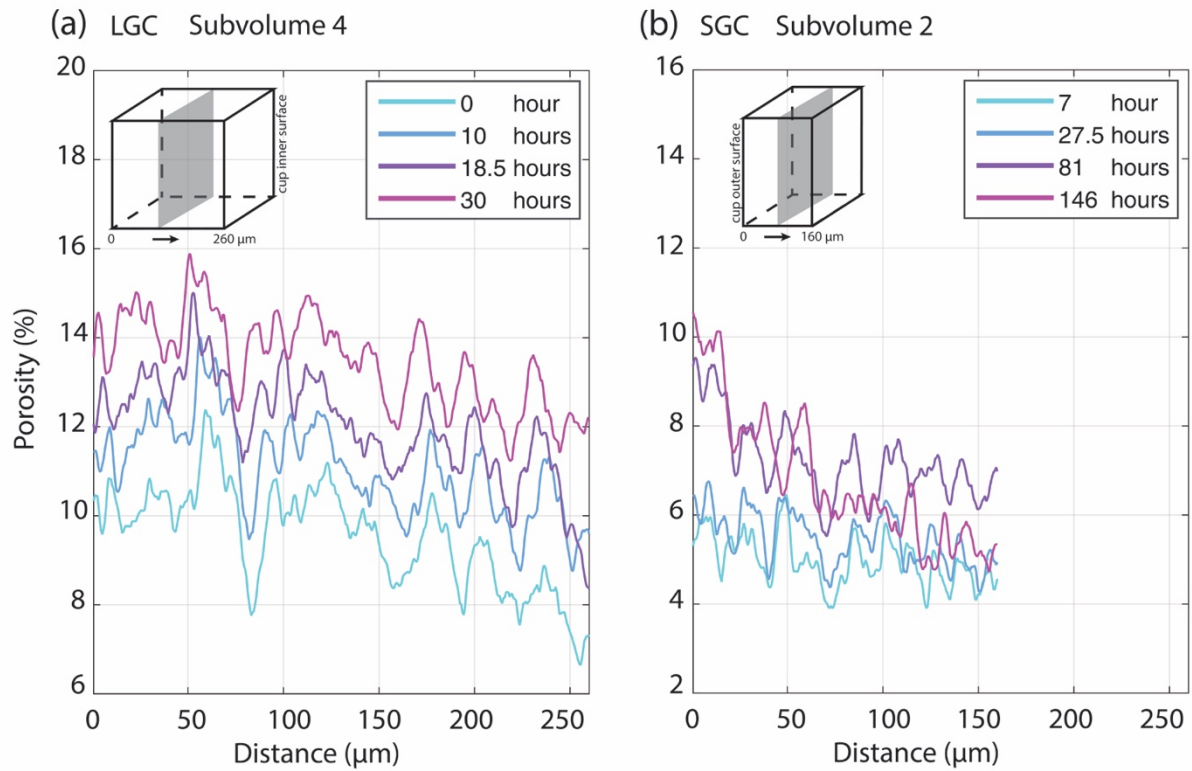
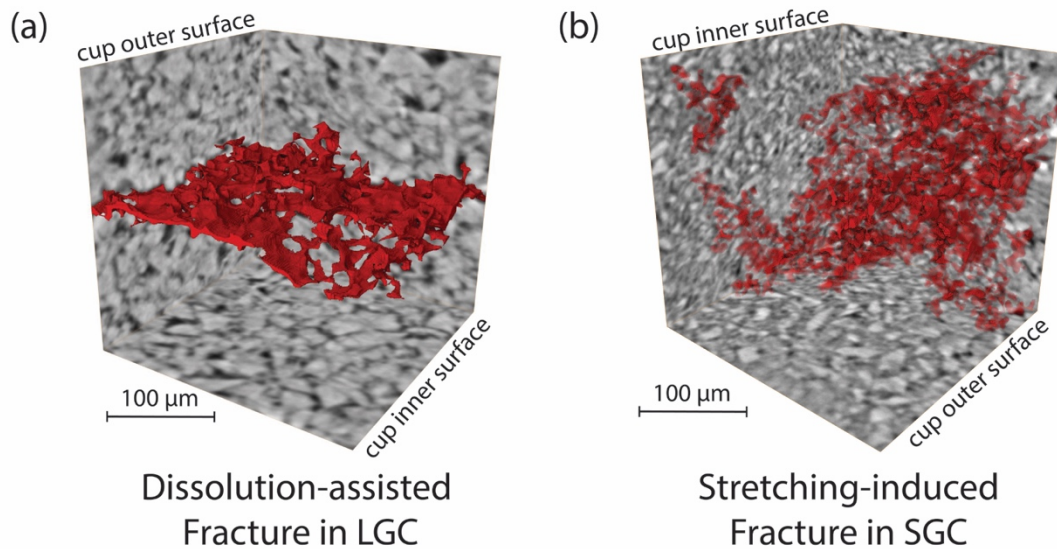


Figure 8: Comparison of porosity evolution in LGC (this study) versus SGC reported by Zhu et al. (2016).

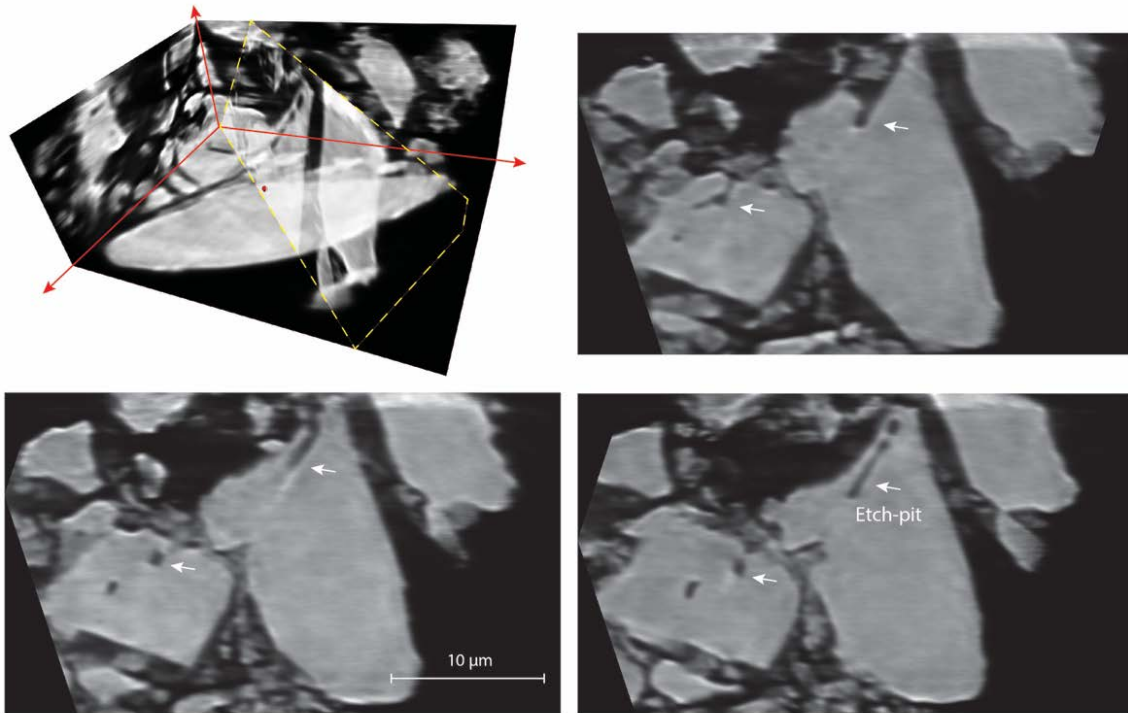


700 **Figure 9: 3D volume Porosity profile of a) LGC and b) SGC along the radial direction of the sample cup. Different colors indicate reaction time lapse.**



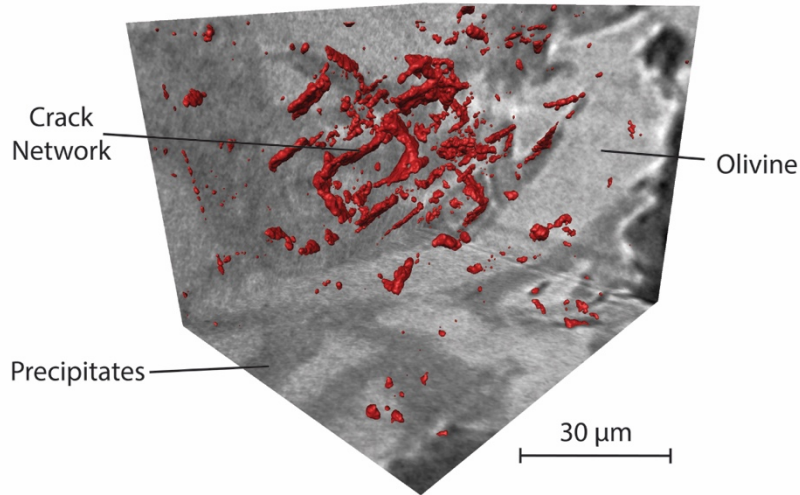
705

Figure 10: The 3D geometry (in red) of a dissolution-assisted fracture network in the fine-grained aggregate and LGC is distinctively different from b) the dissolution feature in the coarse grain aggregate. The fracture network shows a complex of stretching-induced fractures propagating from the surface towards the interior. The dissolution features appear to be planar without the formation of a complex network in SGC. Both displayed volumes are $260 \times 260 \times 260 \mu\text{m}^3$ in size.



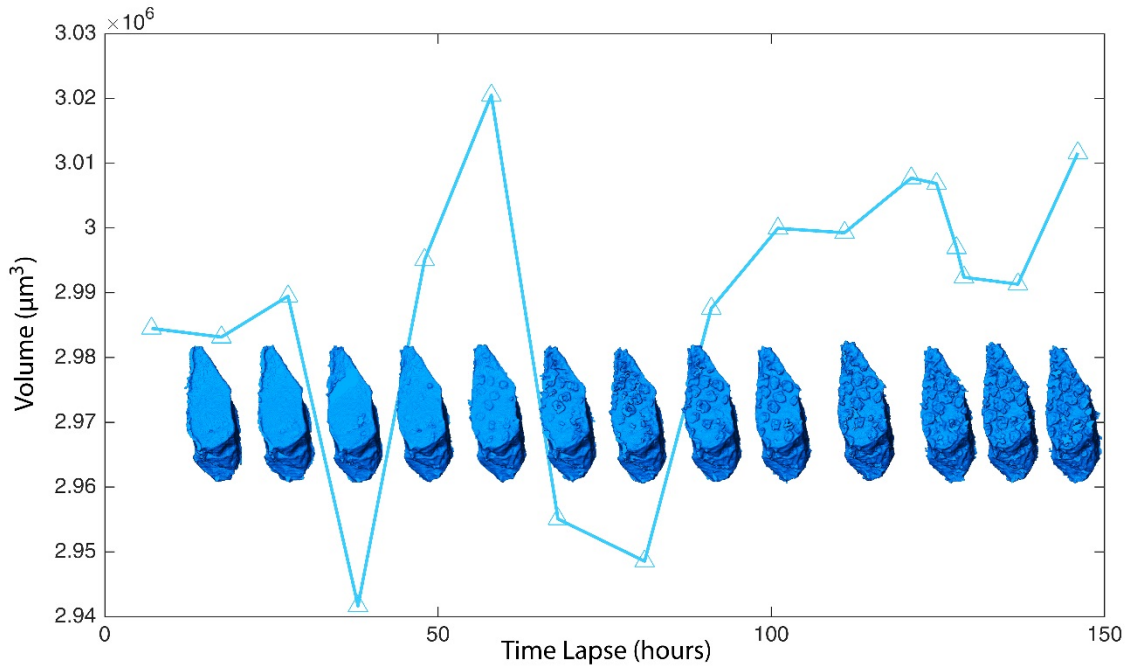
710

Figure 1011: Reconstructed images from the nanotomography data of the SGC sample's cup wall demonstrate the existence of etch-pits and dissolution channels (white arrows) formed in the olivine grain. The precipitates (darker grey) partially fill the pore space (black) between olivine grains (lighter grey). The yellow dash line (in the upper left image) marks the orientation of the cross-sections (right and lower left images). The vertical distance between each 2D cross-section is $\sim 600 \text{ nm}$. Reacting fluid causes a preferential dissolution of the grain which develops small channels that dig into the grain. These features provide a fluid path and eventually break grains, exposing new reactive surfaces.



715

Figure 12: Network of microcracks (red) in the reaction olivine cup wall from SGC shows a polygonal pattern. The dissolution channels make the grain (light grey) more susceptible and a stress concentration is also likely to occur around the etch pits.



720

Figure 13: Volume change of an individual olivine grain (total volume of olivine and precipitates) during carbonation reaction in the SGC experiment. The precipitates are idiomorphic and referred to as magnesites (see Zhu et al., 2016). This observed volume change results from a combination of the dissolution of olivine and precipitation of magnesites. Fluctuations of the grain volume manifest the altering dominance of dissolution versus precipitation.

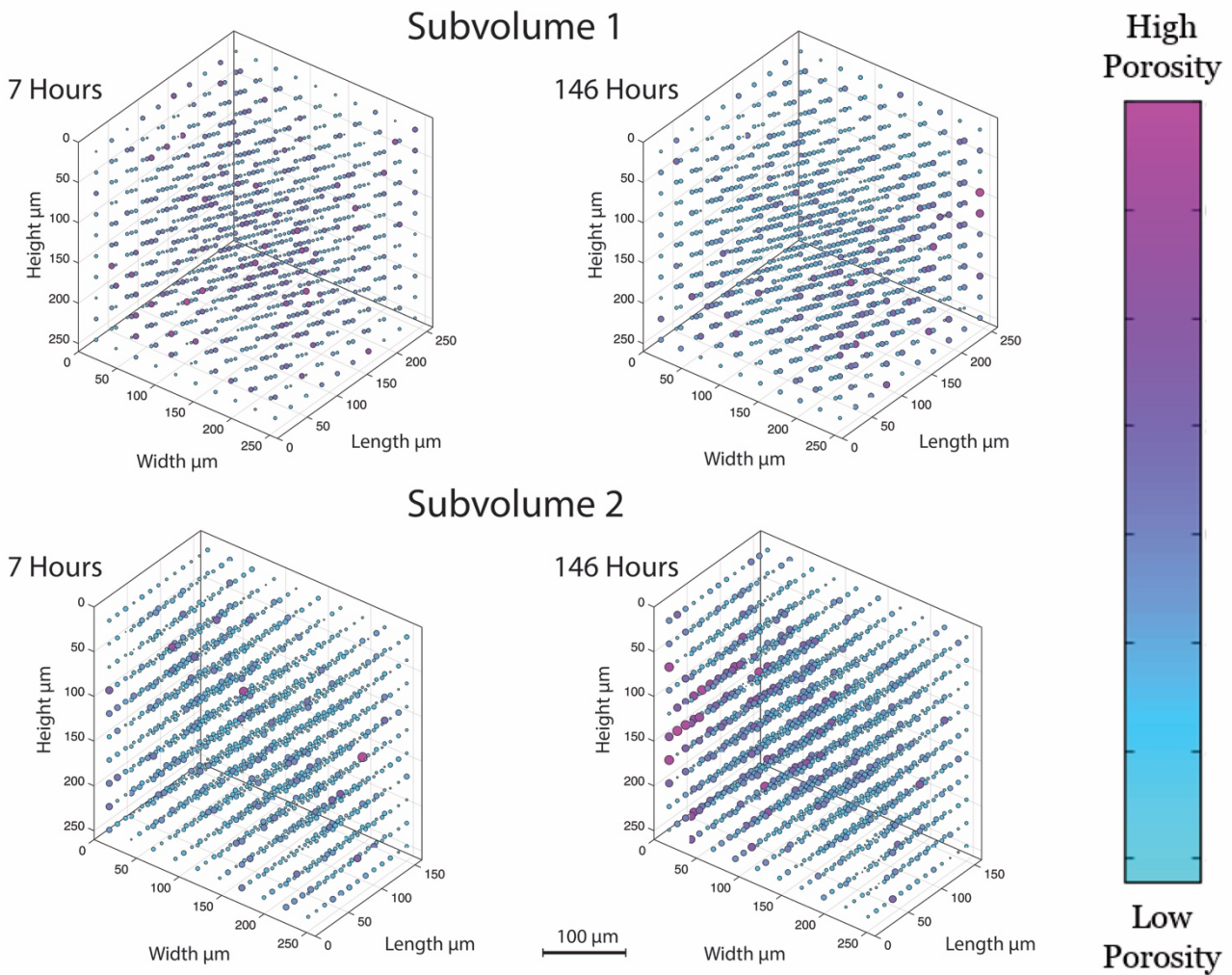
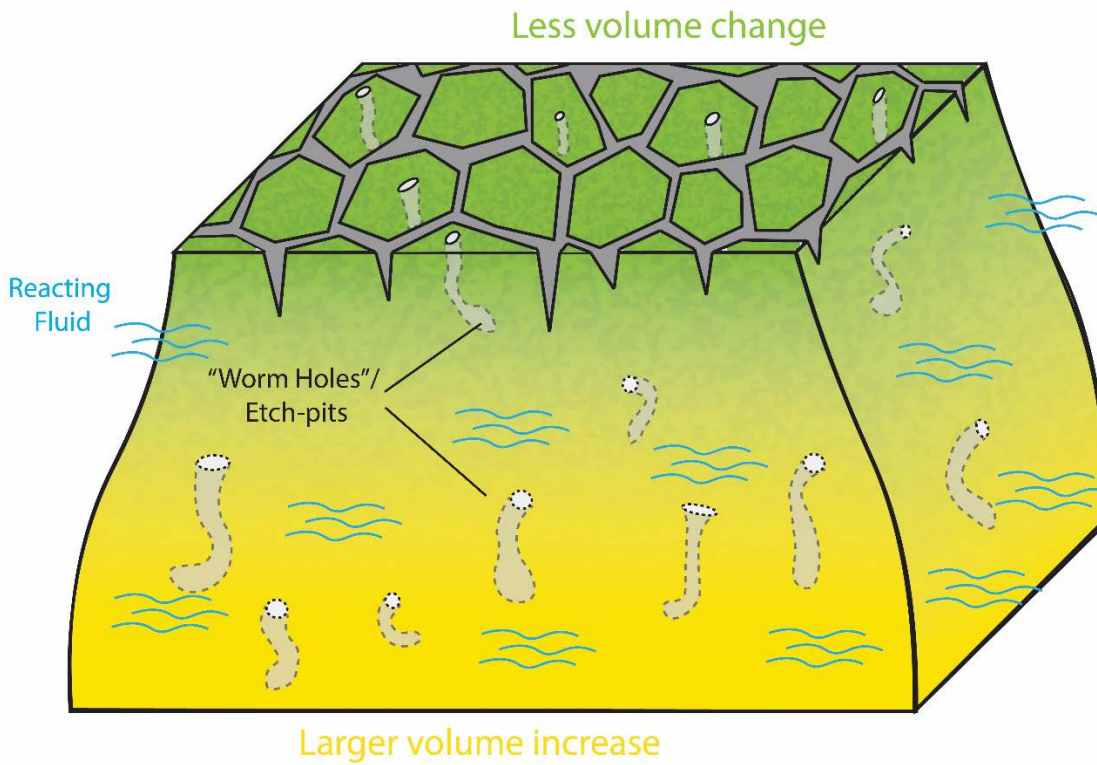


Figure 134: Pores distribution within the subvolumes from SGC sample. For subvolume 1 which contains more inner part of the sample, porosity is relatively homogenous among the volume. For subvolume 2, as it contains more outer part of the sample, a concentration of high porosity can be found in the outer edge compare to the inner edge of the subvolume. This contrast in porosity also reflects a non-uniform precipitation which generates stress that fractures the rock.

725



730 **Figure 1415:** Illustration of porosity generation mechanisms during the olivine carbonation reactions. A combined mechanism of surface cracking and the dissolution channelization plays an important role in the porosity generation. Heterogeneity in the micro-structure of the material would cause ~~non~~non-uniform distribution of precipitation. This would lead to the generation of surface cracking via volume mismatch and generate secondary porosity. Dissolution also produces pore spaces and fluid pathways through etch-pitting channelization which makes the grains susceptible for the cracking on a longer time scale.

735